Iodine dissolution mechanisms in high-pressure aluminoborosilicate glasses and their relationship to oxygen speciation

Yann Morizet, Sami Soudani, Jonathan Hamon, Michael Paris, Carole La, Eric Gautron

IODINE DISSOLUTION MECHANISMS IN HIGH-PRESSURE ALUMINOBOROSILICATE GLASSES AND ITS RELATIONSHIP TO OXYGEN SPECIATION

Yann MORIZET[a*], Sami SOUDANI[a,b], Jonathan HAMON[b], Michael PARIS[b], Carole LA[a], Eric GAUTRON[b],

[a]Nantes Université, Université Angers, Le Mans Université, CNRS, UMR 6112, Laboratoire de Planétologie et Géosciences, F-44000 Nantes, France

[b]Nantes Université, CNRS, Institut des Matériaux de Nantes Jean Rouxel, IMN, F-44000 Nantes, France

*Corresponding author: Yann Morizet

Postal address:

Nantes Université, Université Angers, Le Mans Université, CNRS, UMR 6112, Laboratoire de Planétologie et Géosciences.

2 rue de la Houssinière, 44322 Nantes Cedex (FRANCE)

phone: +33 (0) 2 5112 5491

fax: +33 (0) 2 5112 5268

*E-mail: yann.morizet@univ-nantes.fr

Abstract

Incorporation of iodine (I) into high-pressure vitrified glasses appears to be a potential solution for the immobilization of ^{129}I radioisotopes. Under those conditions, I dissolution is strongly enhanced, however, the impact I dissolution has on the glass structure remains to be determined to assess the matrix durability.

We have studied experimentally the change in I solubility and speciation in a series of sodium aluminoborosilicate glasses (Na_2O ranging from 10 to 40 mol.%) held at 0.25 and 1.0 GPa and 1250°C. As expected, the I solubility increases with pressure conditions, with increasing Na_2O and is positively correlated to the glass optical basicity. The I speciation determined by XPS is changing with the initial loaded source of iodine (either I_2 or I_2O_5) with a predominant iodide form (I^-) in the glass structure.

The investigation of the oxygen environment in the I-bearing glasses using O 1s XPS revealed that I dissolution induces an apparent oxygen loss within the glass structure. This result is consistent with our current view on I dissolution mechanisms. Furthermore, the subsequent simulations of the O 1s XPS spectra suggest that I dissolution consumes non-bridging oxygen to form bridging oxygen. This change in the oxygen speciation points toward an increase in the glass durability that is an important aspect for nuclear waste immobilization.

Introduction

From the valley of radioactive isotope produced by nuclear activities, ^{129}I isotope represents a problematic nuclear waste. ^{129}I is one of the radioisotopes that has a long half-life (i.e. 15.7 My)[1], has a high-mobility in the environment[2-5] and is noxious for the human health[6-8]. Hence, iodine radioisotope is a major troublesome element that requires an adequate, specific solution for its immobilization. Although ^{129}I is produced in small quantity by the nuclear activity, we are requested to propose a reliable matrix to immobilize it in a durable way for environmental,

societal and health considerations. The main difficulty is that iodine cannot be immobilized using a standard borosilicate glass vitrification protocol owing to its strong volatility at high-temperature[9-11].

So far, several countries (i.e. France and UK) have dealt with this nuclear waste by discharging ^{129}I into the sea[11,12]; however, the efficiency of the isotopic dilution into the sea appears limited leading to localized abnormal concentration in ^{129}I[4,5]. Up to now, no ideal solution has been found; however, several matrices have been considered for immobilizing iodine radioisotopes such as: phosphate glasses[13,14], silver-based compounds[15,16], crystalline phases[17-19] or glass-ceramics[20,21]; each of these with their advantages and drawbacks. More recently, a potential reliable solution has been put forward and involves the use of high-pressure syntheses conditions that allows solubilizing iodine in the structure of melt held at high-pressure and high-temperature that is then quenched to a glass. The results obtained with this protocol are encouraging. Jolivet et al.[22] showed that the I solubility is multiplied by almost three orders of magnitude for Low Activity Waste (LAW) aluminoborosilicate glass composition held under high-pressure conditions at 1 GPa in comparison to I solubility obtained for comparable glass composition at ambient pressure[11,23]. For International Simple Glass (ISG) composition that is analogous to the active R7T7 glass used in France[24], Jolivet et al.[22] obtained I solubility close to 1.5 mol.% at 1 GPa.

Unlike other volatile species with application to various domains (i.e. H_2O[25-27] or CO_2[28-33]), our knowledge on the I behavior in glass is lacking microscopic and macroscopic information. Previous experimental studies showed that I solubility is enhanced in more depolymerized borosilicate glass composition[22,34,35]; I solubility is affected by the presence of B_2O_3[35-37]; I solubility is influenced by the nature of network modifying cation (alkalis or alkaline-earth)[34,35,38]. Finally, recent work[34] demonstrated that I solubility increases strongly with the use of oxidized I_2O_5 source as compared to non-oxidized I_2 source. Strangely enough, the

effect of increasing network modifying cations on I solubility is not clearly established for aluminoborosilicate glasses.

At atomic scale, iodine adopts different dissolution mechanisms. The most common iodine form is iodide species (I^-) that is charge compensated by alkalis cation preferentially[23,36,37,39,40]. Morizet et al.[34] also identified other dissolution mechanisms under oxidizing conditions with the presence of iodate species (I^{5+}) and in some particular circumstances periodate species (I^{7+}). Under those oxidizing conditions, the I^{5+} cations form IO_3^- units[41] charge compensated by available alkalis or alkaline-earth cations. In those dissolution mechanisms, both type of species (I^- and IO_3^-) are not bonded to the glass network (Si, Al or B units) but instead occupy the voids in the glass structure induced by the presence of network modifying cations (alkalis or alkaline-earth cations).

Although recent studies significantly improved our current level of knowledge on the iodine behavior in aluminoborosilicate glasses, there are still grey areas that requires additional systematic studies in order to propose a reliable matrix for the immobilization of iodine radioisotopes. For instance, the impact of iodine on the glass structure is not known with certainty, regardless of the iodine form. Previous investigations[22,38] suggested that the iodine dissolution might induce an increase in the glass degree of polymerization; however, there is actually no clear evidence for that. The degree of polymerization can be described by the proportion of Non-Bridging Oxygen (NBO) and Bridging Oxygen (BO)[42-48] species within the glass structure. Whereas it can be calculated for aluminosilicate glasses, the situation is a little more complicated for aluminoborosilicate glasses combining and mixing Si, Al and B subnetworks[49-53]. Obtaining robust evidences on the change in the degree of polymerization is a crucial information as the change in polymerization is a proxy of the glass durability: an increase in glass polymerization will correspond to an increase in the glass durability[54,55].

The increasing degree of polymerization upon iodine dissolution hypothesis is consistent with the fact that alkali cations are consumed for charge compensating the negative charge on I^- or IO_3^- species. Whether there is a clustering between iodine species and alkali cations due to channeling process in the glass structure[56], which could reduce the glass durability is not determined yet. The observed decrease in the glass transition with increasing iodine content[57] is in opposition to an increase in the degree of polymerization of the glass structure. To our knowledge, the work from Morizet et al.[34] is currently the most advanced in the study of the I dissolution. In their work, they propose two chemical reactions for explaining the I dissolution in borosilicate glasses as I^- and IO_3^- and speculating on its impact on the glass structure. They suggest that 1) NBOs are consumed and converted into BOs in agreement with current suggestion and 2) there is a loss in oxygen into the fluid phase. This latter point is surprising and has not been verified owing to experimental difficulties in measuring the composition of the fluid phase after the experiments.

In the present work, we used an experimental approach to investigate the change in I solubility, speciation and dissolution mechanisms on sodium aluminoborosilicate glass compositions that were equilibrated at high-pressure with a I-bearing fluid phase. The recovered glass samples were characterized quantitatively and qualitatively to determine the existence of an oxygen loss and the potential increase in the glass degree of polymerization resulting from the I incorporation.

Experimental method

Starting compositions

In the present work, we investigated a series of sodium aluminoborosilicate glasses: B15NaX with 15 mol.% B_2O_3 and X corresponding to different Na_2O contents ranging from 10 to 40 mol.% Na_2O. Several studied compositions (i.e. B15Na10 and B15Na20) were chosen such as

to represent close analogues to the LAW aluminoborosilicate glass compositions[58,59]. At 30 and 40 mol.% Na_2O the glass compositions do not correspond to a reliable matrix for the immobilization of radioisotopes. Nonetheless, these compositions remain pertinent to study in order to investigate the systematic evolution of the I solubility in nuclear waste glasses as a function of the alkali content for future modelling. In the investigated compositions the Al_2O_3 is kept constant at 5 mol.% and the SiO_2 is progressively replaced by the Na_2O. Studying this glass series has a double aspect: 1) we will evaluate the effect of increasing Na_2O content on the I dissolution, 2) we will study the change in I dissolution along with the change in the polymerizing degree (i.e. decreasing SiO_2).

Starting material were prepared from spec pure powder SiO_2, Al_2O_3, B_2O_3 and Na_2CO_3. The oxide powders were mixed in an agate mortar and ground under ethanol. Each starting powder was poured in a Pt crucible and melted at 1200°C in a box furnace (i.e. a decarbonation step was done at 950°C). The samples were quenched by dropping the bottom of the Pt crucible into a cold-water bath and the recovered sample consists in a clear glass.

High-pressure syntheses

Recovered I-free glasses were crushed and loaded into 2.5-2.9 mm Pt capsule for the high-pressure experiments. Prior to the glass powder (~50 mg), we loaded a known amount of I_2 or I_2O_5 as a source for iodine (~10 mg, see Table 1): between 5 and 12 mol.% I. We loaded a lower amount of I for the 0.25 GPa experiments as we experienced several capsule bursts for this pressure condition at higher I initial charge. Nonetheless, the initial I content is high enough to insure the I saturation during the experiments. After filling, the Pt capsule is welded shut by arc welding.

We conducted the high-pressure experiments in an Oxford-type end-load piston-cylinder apparatus. We used a ¾ inch and a 1 inch pressure plate for the 1 and 0.25 GPa experiments,

152 respectively. We used ¾ and 1 inch talc-Pyrex assemblies for the experiments. The high-
153 pressure assembly consists in an outer talc sleeve, intercalated Pyrex sleeve and graphite
154 furnace with straight walls. The Pt capsules are then placed inside Magnorite© ceramic
155 pieces. For ¾ inch, two Pt capsules (i.e. with the same glass composition loaded with either I_2
156 or I_2O_5) are collated together; for 1 inch, four Pt capsules are collated in the middle part of the
157 assembly. The experimental protocol for the high-pressure experiments has been described in
158 previous works[29]. For 1 GPa, the assembly is pressurized to 1 GPa, the temperature is
159 increased up to 550°C and hold for 5 min to allow materials relaxation, then the final
160 temperature (1250°C) is reached manually. For 0.25 GPa, the assembly is pressurized to 0.5
161 GPa and temperature is increased to 550°C and left 5 min for relaxation, then the final
162 temperature (1250°C) is reached. During the final heating step, the volume relaxation induces
163 a pressure drop down to 0.25 GPa. The run duration for the 1 GPa experiments was set to 2h.
164 Due to rapid graphite furnace degradation during the experiment, the run duration for 0.25
165 GPa experiments could not exceed 30 min. This aspect does not affect our results considering
166 that we still obtain a glass at the end of the low-pressure experiments. During the experiment,
167 the temperature is monitored by a Eurotherm accurate to ±1°C that is connected to a type S
168 thermocouple (Pt-PtRh10). We applied a 10% correction to the pressure to account for
169 internal frictions involved in talc compression. The experiment is stopped by cutting-off the
170 power and the quench is performed isobarically. For ¾ inch experiments, the quench rate is
171 estimated to ~100°C/s in the first 500°C. For 1 inch experiments, the quench rate is lower and
172 estimated to ~70°C/s in the first 500°C. The integrity of the capsule was checked after the
173 experiment. The recovered samples consist in colored (i.e. brown) clear glasses coated all
174 along with an excess iodine indicating that there was an excess an I fluid phase during the
175 experiment. This excess iodine is removed with ethanol and glass pieces are then dried at
176 60°C for a few minutes.

Analytical methods

Scanning Electron Microscopy Energy Dispersive Spectroscopy (SEM EDS)

The major element and iodine concentrations have been determined using Scanning Electron Microscopy with Energy Dispersive Spectrometer (SEM EDS). The glass chips were mounted into epoxy resin plugs polished to 1 µm. Measurements were conducted on a JEOL JSM 5800LV SEM (IMN Jean Rouxel), equipped with a SDD SAMx dispersive spectrometer. The analytical conditions were 15 kV for voltage and 0.5 nA for current. We conducted the acquisitions on a 20 µm spot size to avoid Na loss under the electron beam. At least five scans of 60 s were collected on each sample at different location on the glass chip. We used the following internal standards for quantifying the elements: corundum for Al_2O_3, wollastonite for SiO_2, NaCl for Na_2O, and RbI for I. The B_2O_3 was not quantified in the glasses owing to its low molecular mass. Based on the replicated measurements, we obtain an uncertainty on major element measurements that is better than 5% in relative to the value and comparable to the error reported in previous works on the same analytical equipment[22,34,35]. For the particular case of iodine, the typical error bar based on replicated measurement is better than ±0.2 mol.%. Data in mol.% are provided in Table 1 along with the error that is calculated from the standard deviation of the replicated measurements. The reported error represents the homogeneity in the element distribution within the glass sample.

Laser Ablation Inductively Coupled Plasma Mass Spectrometry (LA-ICP-MS)

The B_2O_3 content in each sample is determined using a Laser Ablation-Inductively Coupled Plasma-Mass Spectrometry (LA-ICP-MS, LPG Nantes). The spectrometer is an ArF excimer laser (193 nm, Analyte G2, Photon Machines) that is coupled to a quadrupole ICP-MS (Varian Bruker 820-MS). The ablation is performed in a HelEx II 2-Volume Cell with He as carrier gas. We used a laser energy density of 4.54 $J.cm^{-2}$ and with a repetition rate of 10 Hz.

The acquisitions were performed in spot mode with a diameter of 110 μm and an estimated depth of 20 μm. Each glass has been analyzed with five acquisitions throughout the sample chip in order to obtain a standard deviation error on the B_2O_3. The acquisition time was set to 30 s., preceded and followed by a 30 s. blank acquisition. The washout time of the ablation cell was approximately 30 s.

LA-ICP-MS acquisition for B_2O_3 content is designed to complement the major element results obtained by SEM EDS. The data is calibrated against several glass samples. We recorded the ^{11}B and ^{27}Al isotopes and this latter one was used as an internal standard. We used the aluminoborosilicate glasses investigated by Jolivet et al.[60] that have been characterized using multiple techniques (SEM EDS, ^{11}B MAS NMR and ICP Optical Emission Spectrometry) for the quantification of B_2O_3. In particular, we used the LJ5 and ISG glasses studied in Jolivet et al.[60] having 25.2 and 16.5 mol.% B_2O_3, respectively. The standard deviation on the measured B_2O_3 is better than 0.6 mol.% for most of the glasses. For B15Na10-0.25GPa-I_2 and B15Na10-0, we obtained a larger error at ±1.3 and 1.4 mol.%, respectively; suggesting a slight heterogeneity in the glass compositions.

X-ray Photoelectron Spectroscopy (XPS)

X-ray Photoelectron Spectroscopy (XPS) measurements were performed on each glass sample to determine the I, O, B, Si and Al signatures. We carried out the XPS analyses on a Kratos Nova spectrometer (IMN Jean Rouxel) using a monochromatic Al Kα radiation operating at 1486.6 eV (15 kV, 20 mA). Due to the insulating nature of the glasses, we used neutralization of the surface. We analyzed glass chips (several mm^2) corresponding to a surface fracture from the bulk of the experimental charge. The surfaces were not prepared and the analyses were conducted on raw glass surfaces, hence avoiding possible surface contamination. The glass chips were loaded into the sample chamber under high-vacuum conditions ($<10^{-8}$ mbar). The spot size on the sample is 300x700 μm^2 area of analyses. We recorded survey spectra at a

pass energy of 160 eV corresponding to an overall instrument resolution of 1.95 eV and a step of 0.5 eV from -5 to 1200 eV. High-resolution spectra of I 3d, O 1s, B 1s, Al 2p, Si 2p and C 1s core levels were recorded. The instrumental resolution was determined to be 0.54 eV at a pass energy of 40 eV using the Fermi edge of the valence band for metallic silver. We used and energy step of 0.1 eV. We acquired the final spectrum with a cycling mode (between 5 and 10 scans on each sample) for each element and we did not observe any modification of each individual acquisition that would suggest an alteration of the glass under the X-ray beam. A few glass chips were analyzed several times for replicated measurements (see Table 2 for B15Na20-0.25GPa-I2 and B15Na20-1GPa-I2 showing two analyses denoted -a and -b). We calibrated the XPS spectra using the adventitious C 1s in the binding energy at 284.8 eV.

Results

Iodine solubility as a function of Na_2O, iodine source, pressure and optical basicity

We show the change in iodine solubility in mol.% I as a function of Na_2O in Figure 1. The corresponding data are given in Table 1 for the mol.% I and Na_2O. As mentioned in Figure 1, the different series are categorized as a function of pressure conditions (0.25 and 1 GPa) and as a function of I source (I_2 and I_2O_5). We clearly observe that increasing Na_2O between 10 and 40 mol.% induces an increase in the I solubility. For instance, the I solubility for B15Na10 glasses is less than 1 mol.% I whereas I solubility reaches almost 6 mol.% I for B15Na40 glasses. In detail, the change in I solubility appears non-linear as a function of Na_2O regardless of the pressure conditions and I source. Each trend has been fitted with a second order polynomial function as a guide for the eye. Surprisingly, in the literature data there has not been much evidences of the increasing I solubility with increasing network modifying cations. Cicconi et al.[36,37] showed that I solubility is weakly influenced by SiO_2 / (SiO_2 + B_2O_3). More recently, Vénague et al.[38] demonstrated that I has higher affinity to Na as compared to other alkalis (K, Li and Cs). In a similar way, Morizet et al.[34] concluded that I is

also preferentially associated to Na as compared to Ca. The experimental studies from Jolivet et al.[22] and Morizet et al.[35] are the only one to show that there is an increase in the I solubility with the increasing concentration of network cations; however, Jolivet et al.[22] worked on different glass compositions that contain both Na and Ca at different ratios. In the present work, we go further and demonstrate that I solubility is positively correlated to the increasing concentration of Na_2O. Interestingly, it would be pertinent to provide comparable experimental evidences for other cations and decide with which cation I has the higher affinity. This question is not entirely answered and is rather complex. It seems there is an interplay between network modifying cations and network forming cations[52].

We also see from the results in Figure 1 that the I solubility is increasing with increasing pressure. This is especially visible for the B15Na30 and B15Na40 glasses. As an example for B15Na30, I solubility is 1.7 mol.% at 0.25 GPa and increases to 2.2 mol.% at 1 GPa. The I solubility increase seems less pronounced for B15Na20 with a change between 0.5 and 0.8 mol.% I from 0.25 and 1 GPa. Previous studies[11,23] reported a solubility of ~0.7 mol.% for comparable glass compositions (25-30 mol.% network modifying cations Na_2O and CaO) synthesized at ambient pressure. The 1.7 mol.% obtained for I solubility in B15Na30 synthesized at 0.25 GPa is almost three times the I solubility obtained at ambient pressure. This result confirms that the application of high-pressure conditions is an adequate solution for the immobilization of ^{129}I radiotoxic isotopes; especially considering that the present experiments performed at 0.25 GPa are feasible from the industrial viewpoint.

We also show that using different I source induces a change in the I solubility. It appears that I solubility is higher in glasses equilibrated with I_2O_5 initial source than in glasses equilibrated with I_2 initial source. The increase in the I solubility from I_2 to I_2O_5 is non-linear with sodium content and appears to be more pronounced for B15Na40 glass. At 1 GPa, we measured a solubility of 4.4 and 5.8 mol.% I for B15Na40 glasses equilibrated with I_2 and I_2O_5 fluid

phase, respectively. Morizet et al.[34] showed the same behavior on a Na-Ca glass series at 1.5 GPa. They ascribed the observed change to the change in I speciation within the glass from I^- to I^{5+} when I_2 or I_2O_5 is used as the I initial source, respectively. However, we will show that it is a little more complicated than the only change in iodine speciation from I^- to I^{5+}.

We also have the reported in Figure 2 the change in the I solubility as a function of the glass optical basicity (Λ_{Glass}) calculated from the major element composition and using the equation of Duffy[61]:

$$\Lambda_{Glass} = \sum \frac{X_i}{\gamma_i} = \sum X_i \times \Lambda_i \qquad \text{Eq. 1}$$

Where X_i corresponds to the molar fraction of oxygen atoms for each oxide and γ_i is the basicity moderating parameters of the oxide i. We took 0.870, 1.613, 1.887 and 2.174 for γ_{Na2O}, γ_{Al2O3}, γ_{SiO2} and γ_{B2O3}, respectively; as reported in Komatsu et al.[62]. It should be pointed out that those values can only approximate the calculation of the Λ_{Glass} considering we do not have access to the change in the glass structure as a function of pressure conditions in the current work. It is currently known that pressure induces a change in the distribution of BO_3 and BO_4 units in the glass structure[35,53,63-65]. Dimitrov et al.[66] reported a $\gamma_{BO4} = 4.17$ and Duffy[67] reported a $\gamma_{BO3} = 2.47$ that would modify the Λ_{Glass} value substantially. Nonetheless, we show that an increase in the Λ_{Glass} is accompanied by an increase in the I solubility. We added the corrected compiled data points from Morizet et al.[35] after we detected a slight miscalculation on the optical basicity values. Ultimately, the Λ_{Glass} could be used as a unique compositional parameter for calculating I solubility in glasses. The Λ_{Glass} is intimately correlated to the nature of the oxygen species within the glass and its electron donation capability[68-70], therefore, by extent, the I solubility in glass should be correlated to the different oxygen species: NBO and BO.

Element spectra obtained by X-ray Photoelectron Spectroscopy (XPS)

Typical XPS spectra obtained on different glasses are shown in Figure 3. All spectra were treated with CasaXPS© software and are represented background subtracted in Figure 3. We fitted the spectra with a U2 Tougaard function as a background[71]. We show XPS spectra for the two glass series: B15NaX I_2 and B15NaX I_2O_5 synthesized at 1 GPa, and for all glass compositions from Na10 to Na40. For each series, we show I $3d_{5/2}$, O 1s, B 1s, Si 2p and Al 2p (Figure 3A-E and Figure 3F-I for B15NaX I_2 and B15NaX I_2O_5, respectively). It should be pointed out that prior to each spectrum simulation, the entire peak area for each element is extracted using CasaXPS© integration module.

The I $3d_{5/2}$ spectra are accompanied with typical spectrum simulations to further discuss the I speciation. The I $3d_{5/2}$ spectra exhibit two or three peaks depending on the I initial source (Figure 3A and F). There is a peak at ~619 eV assigned to I^- species, one at ~621 eV assigned to I^0 species and one at ~624 eV assigned to I^{5+} species. The peak assignment has been described in previous similar studies[34,35,40,41]. The peak for I^{5+} is essentially present in the experiments with I_2O_5 as the initial source and almost absent in the experiments with I_2. In some cases, we observed the presence of I^0 (Figure 3A for B15Na10 and B15Na20). The S/TEM imaging of B15Na20-1GPa-I2 (see Suppl. Mat. 1) did not reveal the presence of nanometer fluid inclusions; therefore, it suggests that the observed I^0 species is actually dissolved in the glass structure. The I $3d_{5/2}$ peaks were fitted with Voigt lines; in some cases we performed peak model testing for the percentage of the Gaussian component to improve the fit of the I^- and I^0 species. The I^{5+} appears well-separated from the two others and the fit was conducted without constraints with a Voigt 30% Gaussian line. The I speciation results expressed as the % of the species are provided in Table 2 and the entire set of simulation can be found in Suppl. Mat. 2. The derived I speciation in Table 2 corresponds to the I speciation in the glass bulk owing to the used XPS beam size. In the current state, we cannot access whether there is a particular segregation of the iodine species that could result from

channeling effect in the glass structure.[56] This aspect is prime importance and requires further investigation as the glass chemical durability could be dramatically affected by such a phenomenon.[72]

The spectra obtained for O 1s, B 1s, Si 2p and Al 2p consist in an almost symmetrical peak located at ~532, ~193, ~103 and ~74 eV binding energy, respectively. The typical simulation obtained for the B 1s, Si 2p and Al 2p is not shown in Figure 3 for clarity. For Si 2p, we fitted the spectra using two Voigt lines with 30% Gaussian component with the same width and separated by 0.61 eV accounting for the $2p_{1/2}$ and $2p_{3/2}$ lines underneath the Si peak. We applied the same procedure for the Al 2p peak and the peak doublet was separated by 0.42 eV. The fitting of the Al 2p spectrum has been complicated by 1) the low spectral signal to noise due to the low Al_2O_3 concentration (see Table 1) and 2) the presence of Pt 4f signal at ~72 eV and ascribed to polluting Pt particles remaining after capsule opening. The B 1s was fitted with a single Voigt line with 30% Gaussian component. The error on the fit obtained from CasaXPS© is dependent on the intensity of the peaks is inherent to the signal to noise ratio. For instance, for the samples with low I content (B15Na10 and B15Na20 glasses) the standard deviation obtained can be as high as 3% on each I species.

In Figure 3, we observe that for O 1s, B 1s and Si 2p the peak position is changing as a function of composition. There is a systematic negative shift in binding energy with increasing Na_2O. This shift is well-documented in previous works and is directly correlated to the change in the glass chemical composition and by extent to the glass optical basicity[35,73-76]. This apparent shift is not visible for I 3d and Al 2p spectra. For Al 2p spectra, this is probably due to the low resolution on the peak. The derived peak positions for Si 2p and B 1s are given in Suppl. Mat. 2. The simulated peak position varies from 102.2 to 103.0 eV for Si $2p_{3/2}$ and from 192.2 to 193.2 eV for B 1s. These changes are above any possible analytical error considering the used XPS resolution (±0.1 eV).

Determining oxygen species from XPS fitting

In the present work, we focused on the change in oxygen concentration and speciation upon I dissolution. We show several typical O 1s spectrum simulations in Figure 4 for all the glass compositions obtained at ambient pressure without iodine: B15Na10-0, B15Na20-0, B15Na30-0 and B15Na40-0. These spectrum simulations represent the starting point for the subsequent simulations of the I-bearing O 1s XPS spectra (see Table 2). At high binding energy (~536 eV) there is a visible peak assigned to the Auger electron of the Na KLL and this peak increases in intensity with increasing Na_2O content as seen in Figure 4. The fit of the O 1s spectra was conducted with several Voigt lines. It should be emphasized that the proposed fit represents only one possible solution and alternative solutions may be considered.

The O 1s XPS spectrum fitting was first conducted on the 1 bar glass O 1s XPS spectrum for each composition considering that these glasses have been used for all the subsequent high-pressure experiments. The simulation procedure has been done as follow: 1) one peak was placed and optimized for the Na Auger, 2) the number of peaks for oxygen species is determined based on the glass composition, 3) the peaks are positioned and optimized according to the current literature knowledge, 4) the simulation obtained on the 1 bar O 1s XPS spectrum is then propagated to the other spectra for the same composition and 5) a new optimization of the peak parameters is conducted for I-bearing glass spectra. Due to the lack of available XPS data for aluminoborosilicate glasses, we applied constraints on the fit. We fixed the FWHM as identical for each category of oxygen species: BO and NBO. It should be emphasized that the proposed approach using the simulation of the O 1s XPS spectra is a first stone and additional work combining O 1s XPS and advanced ^{17}O NMR techniques would be appropriate for investigating the glass O speciation in a thorough way. The entire set of

simulations can be found in the Suppl. Mat. 2 and the change in the proportion of each oxygen species as a function of iodine content is discussed later on.

In the investigated glass compositions, the nature of the expected oxygen species can be determined using the Dell et al.[49] model predictions and subsequent implementation by Du and Stebbins[52] for Al-bearing glasses. The nature of the oxygen species in the aluminoborosilicate glasses can be asserted considering the R' ($[Na_2O] / [Al_2O_3 + B_2O_3]$) and K' ($[SiO_2] / [Al_2O_3 + B_2O_3]$, see Table 1) values of the glass compositions defined by Du and Stebbins[52]:

- For B15Na10, the R' is above 0.5 and the glass composition should have only BO species and we expect no NBO in this glass composition.
- For B15Na20, the R' is comprised between 0.5 and the R'MAX (0.5 + K'/16) for which, in this glass region, there is coexistence between BO and NBO species: $Si\text{-}O^-..Na^+$. We should not expect the presence of $B\text{-}O^-..Na^+$ that corresponds to a NBO linked to a boron species that is necessarily a BO_3.
- For B15Na30 and B15Na40, the R' is above the RD1 (0.5 + K'/4). In this range of glass composition, in addition to the BO species mentioned above, the proportion of NBO increases significantly and there is apparition of $B\text{-}O^-..Na^+$. The excess Na induces the conversion of BO_4 into BO_3 with one or two NBOs.

The simulations obtained in Figure 4 were conducted according to the previous description. The B15Na10-0 exhibits two peaks located at ~532.0 and 532.7 eV that are assigned to two types of bridging oxygen species. For instance, in sodium silicate glasses, Nesbitt et al.[77] proposed the existence of two different BO species: Si-O-Si moiety and BO-Na moiety in which there is a sodium cation located in the BO vicinity. In our study, the story is a little more difficult to apprehend considering that there is a mixing between several subnetworks:

Si- B- and Al-network. Owing to the lack of O 1s XPS data on aluminoborosilicate glasses, we will refer to BO#1 and BO#2 (see Figure 4 and Table 2). The same peaks were found in the other glass compositions with a position and FWHM slightly varying (see Table 2). In between B15Na10-0 and B15Na20-0, we observe an inversion in the peak intensity for the BO#1 and BO#2. This inversion is currently unexplained; however, a difference in the mixing of the structural network units could be the reason for this inversion[51]. The simulation propagation to the I-bearing O 1s spectra of the same glass composition led to similar results suggesting that such inversion is not an analytical artefact but is inherent to the glass composition itself.

Surprisingly, we observe that another peak is required to fully reproduce the spectrum for B15Na10-0 and located at 529.8 eV. According to previous data[77-80], this peak is assigned NBO species and possibly to $Si\text{-}O^{-}..Na^{+}$; although it is not supposed to be present in this glass composition with the Dell et al.[49] model. This peak appears to increase slightly in intensity for B15Na20-0. We expected this peak to increase in intensity for the more depolymerized B15N30-0 and B15N40-0, but it does not seem to be the case. However, for B15N30-0 and B15N40-0 another peak was required and is located at ~531.1 eV and is assigned another type of NBO species that is possibly $B\text{-}O^{-}..Na^{+}$ species[74]. Since B has a higher electronegativity value than Si on the Pauling scale, it implies that B atoms have a higher tendency to attract the oxygen electrons and we expect to find the $B\text{-}O^{-}..Na^{+}$ peak position at higher binding energy. As a result, it explains that $B\text{-}O^{-}..Na^{+}$ peak position is shifted to higher binding energy as compared to the peak position for $Si\text{-}O^{-}..Na^{+}$. In the depolymerized glass compositions, the $B\text{-}O^{-}..Na^{+}$ peak appears more intense than the $Si\text{-}O^{-}..Na^{+}$ peak suggesting that the added Na atoms act preferentially as a network modifier on the B network.

For B15Na30-0 and B15Na40-0, ~16 and ~22% NBOs are expected according to Dell et al.[49] model. As shown in Table 2, the simulation results are overestimated as compared to the

423 model calculation: 34 and 48% NBOs for B15Na30-0 and B15Na40-0, respectively. This
424 could be due to an analytical artefact considering that XPS is a surface analysis method and it
425 has been shown that glass surface has higher concentration in depolymerized network units
426 (i.e. higher NBOs) than the glass bulk itself[81]. Alternatively, it could be related to the way the
427 spectra are simulated and the lack of constraints we have on the position of the different
428 oxygen species. Moreover, it should be emphasized that we cannot preclude from an effect of
429 pressure and/or iodine on the XPS peak parameters.

430 We observed the presence of an additional peak for one I-bearing glass sample: B15Na20-
431 1GPa-I2O5; and located at ~533.8 eV (see Figure 3 and Suppl. Mat. 1 and 2). Currently, the
432 peak assignment is not clear; however, previous data mentioned the presence of Si-OH peak
433 at ~533 eV[81]. Therefore, this peak could correspond to the presence of H_2O in the structure of
434 B15Na20-1GPa-I2O5. As a result, we discarded this sample in the study of the oxygen loss
435 and change of oxygen speciation upon iodine dissolution.

436 **Discussion**

437 *Evolution of the I speciation upon experimental conditions*

438 The change in the I speciation for the different high-pressure experiments is shown in Figure
439 5 and categorized as a function of the glass composition. There are several interesting points
440 to be drawn from the evolution of the I speciation. The first is that using I_2O_5 as an initial
441 source for iodine induces an increase in the I species oxidation state (i.e. I^{5+}). Except for
442 B15Na20-1GPa-I2O5, I^{5+} species can represent more than 28% of the dissolved I and up to
443 63% in B15Na40-1GPa-I2O5. This result is in agreement with the previous study by Morizet
444 et al.[34] demonstrating that I atoms release electron and combine to available O atoms to form
445 IO_3^- clusters within the glass structure[41]. However, the achieved I^{5+} concentrations in the
446 present work are lower than the one reported in Morizet et al.[34] in which I^{5+} can reach up to

447 90% of the total iodine species. We suspect that there is an experimental issue for this
448 difference. In the present work we have used 2.5-2.9 mm diameter Pt capsule whereas
449 Morizet et al.[34] used 5.0-5.4 mm one. It is not clear if this difference affects the I speciation
450 and experimental tests have to be conducted. As mentioned, there is a particular issue with
451 B15Na20-1GPa-I2O5 in which the proportion of I^{5+} is close to 0. We suspect that this sample
452 incorporated H_2O that prevents the conversion of iodine into I^{5+} units.

453 We also see that the proportion of I^0 is important in the B15Na10 glasses with almost up to
454 40% of the I speciation for B15Na10-1GPa-I2. As mentioned earlier, S/TEM did not reveal
455 the presence of nm-size bubbles suggesting that I^0 species are actually dissolved within the
456 glass structure. In complement to the I dissolution mechanisms proposed by Morizet et al.[34],
457 an additional dissolution reaction for I^0 is taking place:

458 $$I_2^{fluid} \leftrightarrow I_2^{melt} \qquad \text{Eq. 2}$$

459 This contrasts with previous assertion in Morizet et al.[40] suggesting that the existence of I^0
460 species was due to the presence of fluid inclusions filled with I_2 because of the excess iodine
461 in the fluid phase during the experiments.

462 *Evidence for O loss upon I dissolution*

463 Recently, Morizet et al.[34] proposed two dissolution mechanisms for I^- and I^{5+} in
464 aluminoborosilicate glasses synthesized under high-pressure conditions, such as:

465 $$\frac{n}{2} I_2^{melt/fluid} + M^{n+}..O_n^{-\,NBO} \leftrightarrow M^{n+}..I_n^- + \frac{n}{2} O_2^{fluid/melt} + \frac{n}{2} O^{BO} \qquad \text{Eq. 3}$$

466 $$\frac{n}{2} I_2^{fluid/melt} + \frac{5n}{2} O_2^{fluid/melt} + M^{n+}..O_n^{-\,NBO} \leftrightarrow M^{n+}..(IO_3^-)_n + \frac{n}{2} O^{BO} \qquad \text{Eq. 4}$$

467 In both chemical reactions, there is a strong interplay between I species and the O species.
468 The net result is to consume NBO species that are converted into BO species due to the

charge compensation of I^- and IO_3^- requirements by Na^+ cations. Those mechanisms imply that I dissolution induces an increase in the degree of polymerization of the glass and therefore potentially increasing durability. Moreover, in Eq. 3 this conversion is also accompanied by an oxygen loss into the fluid phase.

Measuring the composition of the fluid phase after the experiments is complicated and the possible O loss is currently not determined. In the present work, we have tried to determine the change in the O concentration within the glass using the quantitative XPS measurements. Using the total peak areas and the obtained spectrum simulations (see Figure 3 and 4), we have calculated an apparent atomic percentage of oxygen (at.% O) rationalized to either B or Si or the sum of B, Si and Al with the following equation:

$$at.\%\,O = \frac{\frac{A_{O\,1s}}{RSF_{O\,1s}}}{\frac{A_{B\,1s}}{RSF_{B\,1s}}}\ or\ \frac{\frac{A_{O\,1s}}{RSF_{O\,1s}}}{\frac{A_{Si\,2p}}{RSF_{Si\,2p}}}\ or\ \frac{\frac{A_{O\,1s}}{RSF_{O\,1s}}}{\frac{A_{B\,1s}}{RSF_{B\,1s}}+\frac{A_{Si\,2p}}{RSF_{Si\,2p}}+\frac{A_{Al\,2p}}{RSF_{Al\,2p}}} \qquad \text{Eq. 5}$$

In Eq. 5, A_i corresponds to the entire peak area and the RSF is the Relative Sensitivity Factor that is dependent on the element energy line. It should be pointed out that the use of B 1s, Si 2p and Al 2p is justified by the fact that those elements are the network former elements and are the elements that actually carries the different oxygen species. In the investigated glass compositions, the B_2O_3 content is almost constant (see Table 1), hence any variation in the at.% O will be directly related to the change in the oxygen content. Although Al 2p peak intensity is low and not always correctly defined (see Figure 3 and Suppl. Mat. 2), we should rigorously consider it as a network former element.

In a second step, for each glass composition, we normalized the obtained at.% O_i to the at.% O obtained for the initial glass synthesized at 1 bar (at.% O_0) such as:

$$\Delta O_{i/0} = \frac{at.\%\,O_i}{at.\%\,O_0} \qquad \text{Eq. 6}$$

Hence, for initial glasses the $\Delta O_{0/0} = 1$. In doing so, we calculate a variation in the oxygen concentration ($\Delta O_{i/0}$) as compared to the initial oxygen concentration in the pristine ambient pressure glasses. The results are shown in Figure 6 as a function of I content and normalized to all network elements (B 1s Si 2p and Al 2p, Figure 6A), only B 1s (Figure 6B) and only Si 2p (Figure 6C). Data are reported also as a function of the glass compositions. We observe that, invariably, there is a decrease in the $\Delta O_{i/0}$ with increasing I content. It suggests that oxygen is lost upon I dissolution therefore confirming the proposed mechanisms in Morizet et al.[34] for I^- species. Surprisingly, there seems to be also an oxygen loss observed for the samples synthesized with I_2O_5 and exhibiting I^{5+} species. The most important change in the $\Delta O_{i/0}$ is observed for B15Na40 glasses and corresponding to the highest I content. However, there is an outlier with the data point for B15Na10-0.25GPa-I2 in Figure 6C that we do not explain. Except for this particular point, we believe that the observed trends are not issued from any possible analytical or experimental artefacts: 1) the B_2O_3 content is constant therefore the trend observed in Figure 6B reflects the oxygen loss at constant network unit; and 2) the pressure conditions (0.25 and 1 GPa) are identical in between the glass compositions. The $\Delta O_{i/0}$ trends in Figure 6 do not have the same slope (i.e. values) and we suggest that the observed $\Delta O_{i/0}$ only reflects a relative oxygen loss. Intuitively, the $\Delta O_{i/0} < 1$ also suggests that, at constant glass composition, the glass structure polymerizes owing to the rearrangement of the network units upon oxygen loss.

Change in the oxygen speciation as a function of I dissolution

In their work, Morizet et al.[34] suggested that the oxygen speciation should change with NBOs consumed and BOs produced upon the I dissolution. This mechanism corresponds to an increase in the degree of polymerization of the glass that could be beneficial for the durability of the glass for nuclear waste immobilization applications. We have scrutinized the change in the oxygen species based on the spectrum simulations shown in Figure 4. The results are

516 presented in Figure 7 with the % O species as a function of I content and reported for each
517 glass composition. We chose to represent the proportion for each main category of oxygen
518 species (i.e. BO and NBO) considering that the simulated peak assignment is subject to
519 caution. In particular, the nature of each BO species is not clear (see Figure 4). For each glass
520 composition, the plot is represented scaled to the measured I solubility (i.e. the scale is
521 different from one plot to another). The % O species are provided in Table 2. For B15Na10-0
522 glass, the BO concentration is very high (>98%) and the NBO concentration (i.e. $Si\text{-}O^{-}..Na^{+}$)
523 is low (<2%); on the other hand, for B15Na40-0 glass, the BO concentration is lower (<50%)
524 and the NBO concentration (i.e. $Si\text{-}O^{-}..Na^{+}$ + $B\text{-}O^{-}..Na^{+}$) is higher (~50%).

525 As observed in Figure 7, for the most polymerized compositions (i.e. B15Na10 and
526 B15Na20), we observe a slight decrease in the proportion of NBO (i.e. $Si\text{-}O^{-}..Na^{+}$) with
527 increasing I content, accompanied by an increase in the BO proportion. However, this change
528 should be taken with care considering the I solubility range (<0.8 mol.% I) and the associated
529 error bars on the I content (±0.2 mol.%). Nevertheless, it seems to imply that I dissolution
530 involves the NBOs carried by Si networks units for these two glass compositions.

531 For the most depolymerized compositions (B15Na30 and B15Na40), the NBO species
532 concentration decreases with increasing I content and conversely the BO concentration
533 increases. This trend is particularly clear for B15Na40 glasses owing to the high I content
534 measured. The NBO concentration decreases from ~50% to ~30% between 0 and 5.8 mol.% I;
535 in the same time the BO concentration increases from ~50% to ~70% in this I range. For these
536 glass compositions, as shown in Table 2, the NBO-Si species concentration does not change
537 upon I dissolution. Therefore, it suggests that I is preferentially dissolved in the vicinity of the
538 Na^{+} cations associated with boron network ($B\text{-}O^{-}..Na^{+}$) instead of silicon (and aluminum)
539 network. It corroborates the I solubility results of Jolivet et al.[22] suggesting an increase in I

solubility with the presence of B_2O_3 and an extremely low I solubility in pure aluminosilicate glasses.

The results in Figure 7 confirm the previous work of Morizet et al.[34] that suggested the necessary involvement of oxygen species in the I dissolution. In detail, network modifying cations (i.e. Na^+) are scavenged upon I dissolution to charge compensate the I^- and IO_3^- units[23,39-41]. This mechanism requires that NBO species are converted into BO to insure charge neutrality. It implies that the glass degree of polymerization (expressed by the proportion of BO in the glass) increases upon I dissolution.

Previous landmark works showed[82-84] that pressure conditions induce a change in the distribution of the oxygen species in silicate and borosilicate glasses. An increase in pressure will induce a decrease in the NBO concentration. However, this NBO decrease appears to be significant (>10% in relative) at pressure above 3 to 5 GPa and the reported change at pressure of 1 GPa is negligible. Therefore, we suggest that the observed decrease in NBO in Figure 7 is mostly due to the I dissolution, regardless of the pressure conditions (0.25 or 1 GPa).

For more depolymerized aluminoborosilicate glass compositions, we suggest that the $B\text{-}O^-$ ..Na^+ are affected by the I dissolution. We can propose a possible chemical mechanism that have for result to convert a less polymerized boron unit into a more polymerized boron unit:

$$2\,BO_2^{BO} - O^{-NBO} \ldots 2Na^+ + I_2^{fluid} \rightarrow 2NaI + BO_2^{BO} - O^{BO} - BO_2^{BO} + \frac{1}{2}O_2^{fluid} \quad \text{Eq. 7}$$

In the proposed reaction for forming NaI units, there is a conversion of two BO_3 units carrying one NBO into two BO_3 units with no NBO. The literature data acknowledges the existence of both BO_3 units with and without NBO[43,45,49,52,85-87]. This reaction has the advantage to satisfy 1) the loss of oxygen upon iodine dissolution and 2) the increase in the

degree of polymerization. It should be stressed out that in the proposed mechanism there is no creation of fully polymerized BO_4 units and the N_4 ($[BO_4]/[BO_4+BO_3]$, Dell et al.[49]) of the glass is not modified. Again, we should stress out that the proposed mechanism is only possible for glass compositions with available NBO on BO_3 species and corresponding to highly depolymerized glass compositions such as B15Na30 and B15Na40 only. We propose a comparable mechanism for the dissolution of IO_3^- species such as:

$$2\,BO_2^{BO} - O^{-NBO} \ldots 2Na^+ + I_2O_5^{fluid} \rightarrow 2NaIO_3 + BO_2^{BO} - O^{BO} - BO_2^{BO} \quad \text{Eq. 8}$$

In Eq. 8, the I dissolution forms iodate species that are charge compensated by sodium cations: $Na^+..IO_3^-$. There is a conversion between BO_3 units with NBO into BO_3 with only BO, in agreement with the O speciation results in Figure 7; however, an oxygen loss is not requested in Eq. 8. As shown in Figure 5, I is dissolved mostly as I^-, regardless of the initial iodine source (i.e. I_2 or I_2O_5), which implies that both Eq. 7 and 8 are taking place and an oxygen loss should occur.

The results shown in Figure 7 and the derived I dissolution mechanisms from Eq. 7 and 8 constitute a significant breakthrough in the understanding of the iodine effect on the glass structure; however, we still need direct evidences of the iodine impact on the distribution of network units (i.e. silicate Q^n species and boron BO_3 and BO_4 species) to adequately assert the impact of iodine on the glass durability. This aspect is complicated by the fact that the NBOs affected by iodine dissolution is not the same depending on the glass composition: NBO on Q^n species for B15Na20, B15Na30 and B15Na40; NBO on BO_3 species for B15Na30 and B15Na40. Combined approach using ^{11}B, ^{17}O and ^{29}Si Solid-State NMR would be beneficial. Undoubtedly, iodine dissolution increases the glass polymerization. Hence, the range of glass compositions that can be used to serve as an immobilization matrix for iodine radioisotope

would be extended; however, there is a balance to find between the chemical durability and the iodine incorporation that can be achieved.

Conclusion

In the present work, we have investigated the change in I solubility in sodium aluminoborosilicate glasses synthesized under high-pressure conditions at 0.25 and 1 GPa. We studied four different glass compositions at constant B_2O_3 of 15 mol.% and with increasing Na_2O from 10 to 40 mol.% that replaces equally SiO_2. We also investigated the change in the I solubility when various initial source of iodine is used either I_2 or I_2O_5. We show unequivocally that increasing the Na_2O content induces an increase in the I solubility. This result was suspected but has never been clearly demonstrated. It is a crucial information that will be used to point future thermodynamic modelling on the right direction. The I solubility is also increased when I_2O_5 is used as the initial source for iodine, in agreement with previous work. Consistently, I is dissolved under different species with different redox state going from I^- to I^{5+}. We identified that I^0 species measured in glass is actually not corresponding to nanoscale bubbles and an additional dissolution mechanism is proposed to account for the presence of I^0 dissolved in the glass structure.

The detailed quantitative investigation of oxygen using the XPS suggests that there is a loss of oxygen with I dissolution. The decrease in the oxygen concentration has been suspected in previous investigation; however, it has never been clearly demonstrated. The careful scrutiny of the oxygen speciation revealed that the I dissolution is accompanied by a change in the oxygen speciation: the NBO concentration decreases and the BO concentration increases. Those major results support the previous work suggesting the oxygen loss and the conversion of NBO into BO. In addition, it implies that there is an increase in the degree of polymerization of the glass. As an explanation, we propose a reaction that involves the conversion of BO_3 unit with NBO into BO_3 units with no or less NBO. Although very high

alkali aluminoborosilicate glasses are not the most adequate candidate for the immobilization of nuclear waste owing to the lower glass durability, the increase in the glass degree of polymerization accompanying the iodine incorporation is beneficial. Hence, the range of specific reliable/durable glass compositions that can be used for the immobilization of iodine radioisotopes may be extended.

Acknowledgements

The authors are grateful to the Agence Nationale de la Recherche, which financed the current work through the ANR project "Iodine-CLEAN-UP" (ANR-20-CE08-0018). The authors thank the Laboratoire de Planétologie et Géosciences, the Institut des Matériaux de Nantes Jean Rouxel, Nantes Université and the CNRS for providing access to the analytical facilities. The authors thank Nicolas Stephant for its support on the SEM/EDS analytical platform.

References

[1] A. Aldahan, V. Alfimov and G. Possnert, *App. Geochem.*, 2007, **22**, 606–618.

[2] E. Englund, A. Aldahan, X. L. Hou, G. Possnert and C. Söderström, *Nuc. Instr. Meth. Phys. Res. B*, 2010, **268**, 1139–1141.

[3] P. He, X. Hou, A. Aldahan and G. Possnert, *J. Radioanal. Nucl. Chem.*, 2014, **299**, 249-253.

[4] X. Chen, M. Gong, P. Yi, A. Aldahan, Z. Yu, G. Possnert and L. Chen, *Nuc. Inst. Meth. Phys. Res. B*, 2015, **361**, 604–608.

[5] R. Michel, E. Daraoui, M. Gorny, D. Jakob, R. Sachse, L. Tosch, H. Nies, I. Goroncy, J. Herrmann, H. -A. Synal, M. Stocker and V. Alfimov, *Sci. Tot. Env.*, 2012, **419**, 151-169.

[6] C. M. Grossman, W. E. Morton, R. H. Nussbaum, *Arch. Environ. Health*, 1996, **51**, 175–176.

[7] C. M. Grossman, R. H. Nussbaum, F. D. Nussbaum, *Arch. Environ. Health*, 2002, **57**, 9–15.

[8] C. M. Grossman, R. H. Nussbaum, F. D. Nussbaum, *Arch. Environ. Health*, 2003, **58**, 267–274.

[9] P. Hmra, *U.S. department of energy*, Pacific Northwest National Laboratory, 2010, PNNL-19361.

[10] B. J. Riley, J. D. Vienna, D. M. Strachan, J. S. McCloy and J. L. Jr. Jerden, *J. Nuc. Mat.*, 2016 **470**, 307-326.

[11] B. J. Riley, M. J. Schweiger, D. S. Kim, W. W. Lukens, B. D. Williams, C. Iovin, C. P. Rodriguez, N. R. Overman, M. E. Bowden, D. R. Dixon, J. V. Crum, J. S. McCloy and A. A. Kruger, *J. Nuc. Mat.*, 2014, **452**, 178–188.

[12] H. Reithmeier, V. Lazarev, W. Rühm, E. Nolte, *Sci. Tot. Env.*, 2010, **408**, 5052-5064.

[13] A. -L. Chabauty, L. Campayo, F. O. Méar and L. Montagne, *J. Non-Cryst. Solids*, 2019, **510**, 51-61.

[14] A. -L. Chabauty, F. O. Méar, L. Montagne, L. Campayo, *J. Nuc. Mat.*, 2021, **550**, 152919.

[15] X. He, W. Cheng, M. Yan, W. Song, Y. Liu, Z. Zhang, T. Ma, W. Liu, X. Lu, *J. Non-Cryst. Solids*, 2022, 576, 121305.

[16] H. E. Shim, J. E. Yang, S. W. Jeong, C. H. Lee, L. Song, S. Mushtaq, D. S. Choi, Y. J. Choi, J. Jeon, *Nanomat.*, 2018, 8, 660.

[17] L. Campayo, A. Grandjean, A. Coulon, R. Delorme, D. Vantelon and D. Laurencin, *J. Mat. Chem.*, 2011, **21**, 17609.

[18] L. Campayo, S. Le Gallet, D. Perret, E. Courtois, C. Cau Dit Coumes, Y. Grin and F. Bernard, *J. Nuc. Mat.*, 2015, **457**, 63–71.

[19] A. Coulon, D. Laurencin, A. Grandjean, C. Cau Dit Coumes, S. Rossignol, L. Campayo, *J. Mat. Chem. A*, 2014, **2**, 20923–20932.

[20] S. Chong, J.A. Peterson, B.J. Riley, et al., *J. Nuc. Mat.*, 2018, **504**, 109–121.

[21] S. Chong, B.J. Riley, R.M. Asmussen, et al., *J. Nuc. Mat.*, 2020, **538**, 152222.

[22] V. Jolivet, Y. Morizet, M. Paris and T. Suzuki-Muresan, *J. Nuc. Mat.*, 2020, **533**, 152112.

[23] D. A. McKeown, I. S. Muller, I. L., Pegg, *J. Nuc. Mat.*, 2015, **456**, 182–191.

[24] S. Gin, A. Abdelouas, L. J. Criscenti, W. L. Ebert, K. Ferrand, T. Geisler, M. T. Harrison, Y. Inagaki, S. Mitsui, K. T. Mueller, J. C. Marra, C. G; Pantano, E. M. Pierce, J; V. Ryan, J; M. Schofield, C. I. Steefel and J. D. Vienna, *Mater. Today*, 2013, **16**, 243–248.

[25] U. Bauer, H. Behrens, S. Reinsch, E. J. Morin, J. F. Stebbins, *J. Non-Cryst. Solids*, 2017, **465**, 39-48.

[26] H. Behrens, U. Bauer, S. Reinsch, P Kiefer, R. Müller, J. Deubener, *J. Non-Cryst. Solids*, 2018, **497**, 30-39.

[27] S. C. Kohn, *Min. Mag.*, 2000, **64**, 389-408.

677 [28] R. A. Brooker, S. C. Kohn, J. R. Holloway, P. F. McMillan, *Chem. Geol.*, 2001, **174**,
678 225-239.

679 [29] Y. Morizet, R. A. Brooker and S. C. Kohn, *Geochim. Cosmochim. Acta*, 2002, **66**, 1809–
680 1820.

681 [30] Y. Morizet, M. Paris, F. Gaillard and B. Scaillet, *Geochim. Cosmochim. Acta*, 2014, **141**,
682 45-61.

683 [31] Y. Morizet, M. Paris, D. Sifré, I. Di Carlo, S. Ory, F. Gaillard, *Chem. Geol.*, 2017a, **458**,
684 38-47.

685 [32] Y. Morizet, M. Paris, D. Sifré, I. Di Carlo, F. Gaillard, *Geochim. Cosmochim. Acta*,
686 2017b, **198**, 115–130.

687 [33] Y. Morizet, P. Florian, M. Paris, F. Gaillard, *Am. Mineral.*, 2017c, **102**, 1561-1564.

688 [34] Y. Morizet, J. Hamon, C. La, V. Jolivet T. Suzuki-Muresan, M. Paris, *J. Mater. Chem. A*,
689 2021a, **9**, 23902–23915.

690 [35] Y. Morizet, M. Paris, J. Hamon, C. La, S. Grolleau, T. Suzuki-Muresan, *J. Mat. Sci.*,
691 2022a, **57**, 16600–16618.

692 [36] M. R. Cicconi, E. Pili, L. Grousset and D. R. Neuville, *Mat. Res. Soc.*, 2019a, **4**, 17-18.

693 [37] M. R. Cicconi, E. Pili, L. Grousset, P. Florian, J. C. Bouillard, D. Vantelon and D. R.
694 Neuville, *Sci. Rep.*, 2019b, **9**, 7758.

695 [38] B. Vénague, L. Campayo, M. J. Toplis, T. Charpentier, M. Moskura, J. L. Dussossoy, *J.*
696 *Non-Cryst. Solids*, 2022, **576**, 121278.

697 [39] I. S. Muller, D. A. McKeown and I. L. Pegg, *Proc. Mater. Sci.*, 2014, **7**, 53–59.

[40] Y. Morizet, V. Jolivet, N. Trcera, T. Suzuki-Muresan and J. Hamon, *J. Nuc. Mat.*, 2021b, **553**, 153050.

[41] Y. Morizet, N. Trcera, T. Suzuki-Muresan, S. Soudani, E. Fonda, M. Paris, *J. Chem. Phys.*, 2022b, **156**, 154508.

[42] L. Cormier, O. Majérus, D. R. Neuville, G. Calas, *J. Am. Cer. Soc.*, 2006, **89**, 13-19.

[43] F. Angeli, T. Charpentier, D. De Ligny and C. Cailleteau, J. Am. Cer. Soc., 2010, 93, 2693–2704.

[44] F. Angeli, O. Villain, S. Schuller, S. Ispas, T. Charpentier, *Geochim. Cosmochim. Acta*, 2011, **75**, 2453-2469.

[45] J. de Bonfils, S. Peuget, G. Panczer, D. de Ligny, S. henry, P. Y. Noël, A. Chenet, B. Champagnon, *J. Non-Cryst. Solids*, 2010, 356, 388-393.

[46] S. Peuget, E. A. Maugeri, T. Charpentier, C. Mendoza, M. Moskura, T. Fares, O. Bouty and C. Jégou, *J. Non-Cryst. Solids*, 2013, **378**, 301-312.

[47] L. M. Thompson and J. F. Stebbins, *Am. Mineral.*, 2011, **96**, 841-853.

[48] J. Wu and J. F. Stebbins, *J. Non-Cryst. Solids*, 2009, **355**, 556-562.

[49] W. J. Dell, P. J. Bray and S. Z. Xiao, *J. Non-Cryst. Solids*, 1983, **58**, 1-16.

[50] L. S. Du and J. F. Stebbins, *J. Non-Cryst. Solids,* 2003a, **315**, 239-255.

[51] L. S. Du and J. F. Stebbins, *Chem. Mat.*, 2003b, **15**, 3913-3921.

[52] L. S. Du and J. F. Stebbins, *J. Non-Cryst. Solids*, 2005, **351**, 3508–3520.

[53] L. S. Du, J. Allwardt, B. C. Schmidt, J. F. Stebbins, *J. Non-Cryst. Solids,* 2004, **337**, 196-200.

719 [54] F. Angeli, T. Charpentier, P. Jollivet, D. de Ligny, M. Bergler, A. Veber, S. Gin, H. Li,
720 *Nature Mater. Degrad.*, 2018, **2**, 31.

721 [55] D. Caurant, O. Majérus, Encyclopedia of Materials: Technical Ceramics and Glasses,
722 2021, 2, Elsevier, Oxford, 762-790.

723 [56] C. Le Losq, D. R. Neuville, W. Chen, P. Florian, D. Massiot, Z. Zhou, G. N. Greaves,
724 *Sci. Rep.*, 2017, **7**, 16490.

725 [57] V. Jolivet, Y. Morizet, J. Hamon, M. Paris and T. Suzuki-Muresan, *J. Am. Cer. Soc.*,
726 2021, **104**, 1360-1369.

727 [58] I. Muller, I. L. Pegg, M. Chaudhuri, I. Joseph, K. Gilbo, *U.S. department of energy*,
728 Office of the River Protection, 2018, ORP-63490.

729 [59] G. F. Piepel, S. K. Cooley, J. D. Vienna and J. V. Crum, *U.S. department of energy*,
730 Pacific Northwest National Laboratory, 2015, PNNL-24391.

731 [60] V. Jolivet, L. Jossé, M. Rivoal, M. Paris, Y. Morizet, C. La and T. Suzuki-Muresan, *J.*
732 *Non-Cryst. Solids*, 2019, **511**, 50-61.

733 [61] J. A. Duffy, *J. Non-Cryst. Solids,* 1986, **86**, 149–160.

734 [62] T. Komatsu, V. Dimitrov, T. Tasheva, T. Honma, *Int. J. Appl. Glass Sci.*, 2021, **12**, 424–
735 442.

736 [63] S. Kapoor, L. Wondraczek, M. M. Smedskjaer, *Frontiers Mat.*, 2017, **4**, 1.

737 [64] M. Smedskjaer, R. E. Youngman, S. Striepe, M. Potuzak, U; Bauer, J. Deubener, H.
738 Behrens, J. C., Mauro, Y. Yue, *Sci. Rep.*, 2014, **4**, 3770.

739 [65] L. Wondraczek, S. Sen, H. Behrens, R. E. Youngman, *Phys. Rev. B*, 2007, **76**, 014202.

740 [66] V. Dimitrov, T. Komatsu, T. Tasheva, *J. Chem. Tech. Metall.*, 2018, **53**, 1038-1046.

741 [67] J. A. Duffy, *J. Phys. Chem. A*, 2006, **110**, 13245–13248.

742 [68] J. A. Duffy and M. D. Ingram, *J. Non-Cryst. Solids*, 1976, 21, 373-410.

743 [69] V. Dimitrov, S. Sakka, *J. App. Phys.*, 1996, **79**, 1736–1740.

744 [70] V. Dimitrov and T. Komatsu, *J. Chem. Tech. Metall.*, 2015, **50**, 387-396.

745 [71] S. Tougaard, *Surf. Inter. Anal.*, 1997, **25**, 137-154.

746 [72] D. Caurant, O. Majérus, Reference Module in Materials Science and Materials
747 Engineering, Elsevier, Oxford, 2021.

748 [73] W. M. Mullins, *Surf. Sci. Lett.*, 1992, **262**, 144-146.

749 [74] C. H. Hsieh, H. Jain, A. C. Miller, E. I. Kamitsos, *J. Non-Cryst. Solids*, 1994, 168, 247-
750 257.

751 [75] T. Honma, R. Sato, Y. Benino, T. Komatsu, V. Dimitrov, *J. Non-Cryst. Solids*, 2000,
752 **272**, 1–13.

753 [76] Y. Miura, H. Kusano, T. Nanba, S. Matsumoto, *J. Non-Cryst. Solids*, 2001, **290**, 1-14.

754 [77] H. W. Nesbitt, G. S. Henderson, G. M. Bancroft, R. Ho, *J. Non-Cryst. Solids*, 2015a,
755 **409**, 139–148.

756 [78] H. W. Nesbitt, G. M. Bancroft, G. S. Henderson, R. Ho, K. N. Dalby, Y. Huang, Z. Yan,
757 *J. Non-Cryst. Solids*, 2011, 357, 170-180.

758 [79] H. W. Nesbitt, G. M. Bancroft, G. S. Henderson, R. Sawyer, R. A. Secco, *Am. Mineral.*,
759 2015b, **100**, 2566–2578.

760 [80] R. Sawyer, H. W. Nesbitt, G. M. Bancroft, Y. Thibault, R. A. Secco, *Can. J. Chem.*,
761 2015, **93**, 60-73.

762 [81] B. Roy, F. Baier, A. Rosin, T. Gerdes, S. Schafföner, *Int. J. App. Glass Sci.*, 2022, **14**,
763 229-239.

764 [82] S. K. Lee, *Solid State Nuc. Mag. Res.*, 2010, **38**, 45-57.

765 [83] S. K. Lee, *Proc. Nat. Acad. Sci.*, 2011, **108**, 6847-6852.

766 [84] A. C. Lee, E. J. Kim, S. K. Lee, *Geochim Cosmochim. Acta*, 2022, **332**, 220-238.

767 [85] J. Zhong and P. J. Bray, *J. Non-Cryst. Solids*, 1989, **111**, 67-76.

768 [86] S. Sen, Z. Xu, J. F. Stebbins, *J. Non-Cryst. Solids*, 1998, **226**, 29-40.

769 [87] J. F. Stebbins, P. Zhao, S. Kroeker, *Solid State Nuc. Mag. Res.*, 2000, **16**, 9-19.

770

771 **Figure caption**

772 Figure 1: Change in the I solubility as a function of Na_2O content ranging from 10 to 40
773 mol.%. Several datasets are represented with the different experimental conditions: 1 GPa I_2,
774 1 GPa I_2O_5 and 0.25 GPa I_2. It is noticed that small quench crystals were observed for
775 B15Na30 and B15Na40 recovered glasses. The error on the I solubility is ±0.2 mol.%; the
776 error on the Na_2O content is not reported for clarity but can be found in Table 1.

777 Figure 2: The change in I solubility in the investigated glass compositions is represented using
778 the glass optical basicity (Λ_{Glass}). An increase in the Λ_{Glass} corresponds to an increase in the I
779 solubility in agreement with the recent suggestion by Morizet et al.[35]. We also added the data
780 from Morizet et al.[35] acquired on a wide compositional range of aluminoborosilicate glasses.

781 Figure 3: A-E, Typical XPS spectra for glasses obtained with I_2 loaded during the
782 experiments; F-J, Typical XPS spectra for glasses obtained with I_2O_5 loaded during the
783 experiments. We show the spectra for I $3d_{5/2}$, O 1s, B 1s, Si 2p and Al 2p. Typical simulations

784 are shown for the I $3d_{5/2}$ for I speciation. The spectra obtained for Al 2p are usually not well-
785 defined due to the low Al_2O_3 concentration and also show the presence of polluting Pt 4f
786 coming from the capsule walls.

787 Figure 4: Typical O 1s XPS spectrum fitting for the obtained glasses at ambient pressure
788 without I: A, B15Na10-0; B, B15Na20-0; C, B15Na30-0; D, B15Na40-0. The whole set of
789 fitting can be found in the Suppl. Mat. 2. The spectra are best fitted with three to four
790 Gaussian lines for O species and an additional line for Na Auger signal. The proposed
791 assignment for the peaks is the following: ~532.5 and ~532.0 eV to BO#2 and BO#1; ~529.5
792 eV to $Si\text{-}O^{-}..Na^{+}$; ~531.0 eV to $B\text{-}O^{-}..Na^{+}$.

793 Figure 5: Change in the I speciation (I^{-}, I^{0} and I^{5+}) for each glass sample as measured by XPS
794 and subsequent simulation of the I $3d^{5/2}$ spectrum peak. The plot is categorized as a function
795 of the glass composition. There is an increasing concentration of I^{5+} species when I_2O_5 is used
796 as the starting source of iodine in the experiments.

797 Figure 6: Change in the oxygen concentration in glasses expressed as the $\Delta O_{i/0}$ as a function
798 of I content in mol.%. The apparent at.% O_i is calculated in different ways (see text for
799 details): A) rationalized to the sum of the network forming elements (B, Si and Al), B)
800 rationalized to B and C) rationalized to Si. The change in oxygen concentration is then
801 normalized to the oxygen concentration measured in the precursor glasses obtained at 1 bar,
802 such as: $\Delta O_{i/0}$ = at.% O_i / at.% O_0.

803 Figure 7: Change in oxygen speciation as a function of I content in mol.%. The % O species is
804 obtained from the simulation of the O 1s spectra. The two main categories of oxygen species
805 are represented: BO and NBO. The plots are shown for each glass composition. We did not
806 represent the error bars on the I content (±0.2 mol.%) and the slight decrease in NBO
807 concentration for B15Na10 and B15Na20 glass compositions is subject to caution.

808

Table 1: Experimental conditions, major element and iodine concentrations determined by SEM EDS and LA ICP MS.

Sample	Pressure (GPa)	$I^{init.}$ (mol.%)[a]	Major element concentration (mol.%)[b]					Λ_{Glass}[c]	R'[c]	K'[c]
			SiO_2	B_2O_3	Al_2O_3	Na_2O	I			
B15Na10-0	0.0001	0	64.8(14)	18.0(14)	5.9(8)	11.3(7)	0	0.553	0.471	2.713
B15Na10-0.25GPa-I2	0.25	5.2	70.7(6)	16.1(13)	5.6(3)	7.6(4)	0.1	0.543	0.353	3.258
B15Na10-1GPa-I2	1	10.3	72.1(2)	13.9(2)	5.4(1)	8.7(2)	0.3	0.549	0.450	3.738
B15Na10-1GPa-I2O5	1	9.2	70.9(2)	13.8(13)	5.3(1)	10.0(2)	0.6	0.553	0.521	3.704
B15Na20-0	0.0001	0	63.2(6)	14.9(6)	4.2(3)	17.7(3)	0	0.575	0.926	3.306
B15Na20-0.25GPa-I2	0.25	5.2	62.7(3)	14.0(2)	5.3(1)	17.9(3)	0.5	0.578	0.926	3.239
B15Na20-1GPa-I2	1	12.0	61.9(2)	14.0(1)	5.9(1)	18.2(3)	0.8	0.579	0.916	3.111
B15Na20-1GPa-I2O5	1	11.3	63.8(3)	14.2(1)	5.2(1)	16.8(3)	1.4	0.574	0.864	3.284
B15Na30-0	0.0001	0	51.8(4)	14.8(2)	4.8(1)	28.5(4)	0	0.613	1.454	2.643
B15Na30-0.25GPa-I2	0.25	5.3	53.2(4)	13.3(1)	5.4(0)	28.1(3)	1.7	0.614	1.504	2.850
B15Na30-1GPa-I2	1	10.4	57.2(15)	13.7(1)	6.0(1)	23.1(13)	2.2	0.596	1.169	2.896
B15Na30-1GPa-I2O5	1	10.9	55.6(6)	13.5(1)	5.9(1)	24.9(7)	2.6	0.603	1.284	2.865
B15Na40-0	0.0001	0	44.7(13)	13.9(1)	6.5(3)	34.9(16)	0	0.640	1.711	2.191
B15Na40-0.25GPa-I2	0.25	5.6	43.7(3)	12.1(1)	5.7(1)	43.7(3)	3.2	0.657	2.153	2.451
B15Na40-1GPa-I2	1	9.6	45.4(11)	12.4(1)	6.2(2)	36.1(10)	4.4	0.647	1.939	2.439
B15Na40-1GPa-I2O5	1	10.2	46.7(10)	12.7(2)	6.3(2)	34.4(4)	5.8	0.640	1.811	2.461

[a] The I^{init} corresponds to the loaded initial iodine content prior the high-pressure experiment and using different iodine sources: I_2 or I_2O_5.

[b] The major element concentrations have been determined using SEM EDS for SiO_2, Al_2O_3, Na_2O and I; and using LA ICP MS for the quantification of B_2O_3 (see text for details). The reported errors between brackets correspond to the error on the last or two last figures. Error has been determined from the standard deviation calculated from several measurements (at least five acquisitions by SEM EDS and LA ICP MS).

[c] The Λ_{Glass} is calculated from the equation of Duffy[60] (see text for details). The R' and K' values are calculated from the glass chemical compositions and correspond to $[Na_2O] / [Al_2O_3 + B_2O_3]$ and $[SiO_2] / [Al_2O_3 + B_2O_3]$, respectively.

Table 2: Iodine speciation, oxygen concentration and speciation, and XPS fitting parameters.

Sample	I (mol.%)	I 3d$_{5/2}$ [a]						O 1s [b]								$\Delta O_{i/0}$ = at.% O_i / at.% O_0 [c]		
		I^-		I^0		I^{5+}		BO#1		BO#2		Si-O^-..Na^+		B-O^-..Na^+		Norm. to B 1s	Norm. to Si 2p	Norm. to B 1s + Si 2p + Al 2p
		Pos/FWHM	%	Pos/FWHM	%	Pos/FWHM	%	Pos/FWHM	%	Pos	%	Pos/FWHM	%	Pos	%			
B15Na10-0	0							532.4/1.7	68.5(12)	531.5	29.7(11)	529.8/1.2	1.8(2)			1	1	1
B15Na10-0.25GPa-I2	0.1	619.0/1.4	94.0(25)	621.2	6.0(25)			532.5/1.7	81.5(8)	531.4	17.5(7)	529.7/1.2	1.0(1)			0.94	0.99	1.01
B15Na10-1GPa-I2	0.3	619.1/2.0	62.6(29)	621.6	37.4(29)			532.5/1.7	79.4(10)	531.4	18.9(9)	529.8/1.3	1.7(2)			1.042	0.894	0.841
		619.2/1.8	62.8(34)	621.6	37.2(34)			532.5/1.7	84.3(14)	531.5	14.3(13)	529.9/1.3	1.4(3)			0.955	0.996	1.028
B15Na10-1GPa-I2O5	0.6	619.0/1.5	37.2(24)	621.4	21.1(15)	624.1/1.9	41.7(31)	532.3/1.7	79.4(9)	531.3	19.8(9)	529.6/1.1	0.9(1)			1.02	1.02	0.99
B15Na20-0	0							532.4/1.7	23.8(2)	531.6	73.3(2)	529.7/1.2	2.9(2)			1	1	1
B15Na20-0.25GPa-I2-a	0.5	619.2/1.3	99.1(1)	621.5	0.9(1)			532.3/1.8	26.2(3)	531.7	71.4(4)	529.7/1.1	2.3(4)			0.81	1.07	1.09
B15Na20-0.25GPa-I2-b		619.1/1.4	89.5(24)	621.5	10.5(24)			532.2/1.8	54.8(3)	531.6	43.2(3)	529.7/1.1	2.0(2)			0.97	0.93	1.03
B15Na20-1GPa-I2-a	0.8	619.2/1.4	85.0(14)	621.6	15.0(14)			532.2/1.7	49.8(2)	531.6	47.7(2)	529.8/1.2	2.6(2)			1.07	0.83	0.94
B15Na20-1GPa-I2-b		619.1/1.5	87.7(13)	621.3	12.3(13)			532.3/1.8	45.3(3)	531.7	52.6(4)	529.8/1.4	2.1(2)			0.91	0.83	0.92
B15Na20-1GPa-I2O5[d]	1.4	619.0/1.6	89.8(33)	620.9	5.5(12)	624.5/1.8	4.7(27)											
B15Na30-0	0							532.3/1.9	15.2(8)	531.8	50.7(15)	529.8/1.4	2.0(2)	531.2	32.1(7)	1	1	1
B15Na30-0.25GPa-I2	1.7	619.0/1.4	95.6(9)	621.0	4.4(9)			532.5/1.9	7.5(5)	531.8	62.6(13)	529.8/1.3	4.1(2)	531.3	25.9(7)	0.76	0.87	0.83
B15Na30-1GPa-I2	2.2	619.2/1.5	90.8(11)	621.2	4.0(3)	624.2/1.5	5.1(8)	532.3/1.9	10.8(13)	531.8	69.9(23)	529.9/1.4	3.6(2)	531.3	15.7(17)	0.46	0.80	0.76
B15Na30-1GPa-I2O5	2.6	619.0/1.4	68.7(3)	621.0	3.0(2)	624.1/1.3	28.3(2)	532.3/1.9	14.2(7)	531.7	60.1(15)	529.8/1.4	2.8(2)	531.2	22.9(7)	0.62	0.85	0.70
B15Na40-0	0							532.7/1.5	7.6(3)	531.5	44.0(7)	529.6/1.2	1.2(2)	531.0	47.2(5)	1	1	1
B15Na40-0.25GPa-I2	3.2	619.1/1.3	98.6(3)	621.3	1.4(3)			533.0/1.6	6.3(2)	531.6	64.2(4)	529.9/1.2	3.0(2)	531.1	26.5(4)	0.13	1.31	0.48
B15Na40-1GPa-I2	4.4	619.1/1.3	97.1(6)	621.2	1.4(3)	624.1/1.0	1.5(4)	533.1/1.5	7.8(2)	531.7	65.5(5)	529.9/1.2	3.8(1)	531.1	22.9(3)	0.19	0.51	0.39
B15Na40-1GPa-I2O5	5.8	619.0/1.3	33.5(4)	621.2	4.0(4)	624.1/1.3	62.5(5)	532.8/1.6	9.2(2)	531.6	63.5(5)	529.8/1.2	3.7(2)	531.0	23.6(5)	0.19	0.39	0.33

[a] The I speciation has been determined with the simulations of the XPS spectra on the I 3d$_{5/2}$ binding energy. For I^- and I^0 species the peak width has been set as identical. The error on the species percentages is obtained from CasaXPS© fitting results.

[b] The oxygen speciation has been determined from the simulations of the XPS spectra on the O 1s peak. Two peaks for BO species and two peaks for NBO species were found. For each category of oxygen species, the peak width was set as identical. The procedure for fitting the O 1s spectra is fully described in the text. The error on the species percentages is obtained from CasaXPS© fitting results.

[c] The $\Delta O_{i/0}$ corresponds to the ratio between the at.% O_i and the at.% O_0 considered at a reference point (i.e. 1 bar). The at.% O is calculated from the O 1s peak area that is normalised either to B 1s, or Si 2p or B 1s + Si 2p + Al 2p peak areas.

[d] For this particular sample, the O 1s peak showed the presence of an additional component located at ~533 eV and assigned to hydroxyl species. This sample has been discarded in the oxygen speciation determination and oxygen loss.

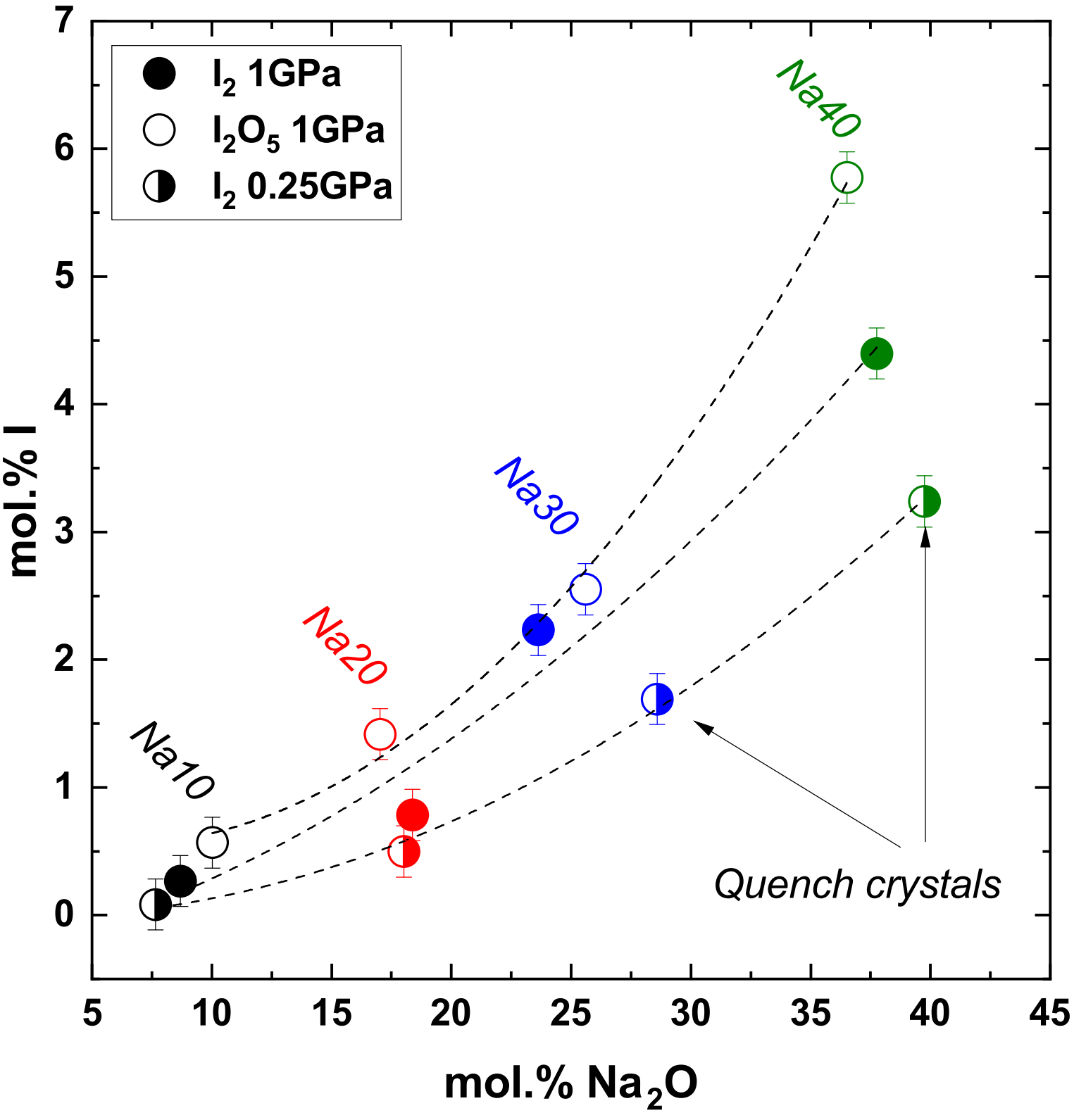
I2 1GPa
I2O5 1GPa
I2 0.25GPa
Na40
Na30
Na20
Na10
Quench crystals
mol.% I
mol.% Na2O
0
1
2
3
4
5
6
7
5
10
15
20
25
30
35
40
45

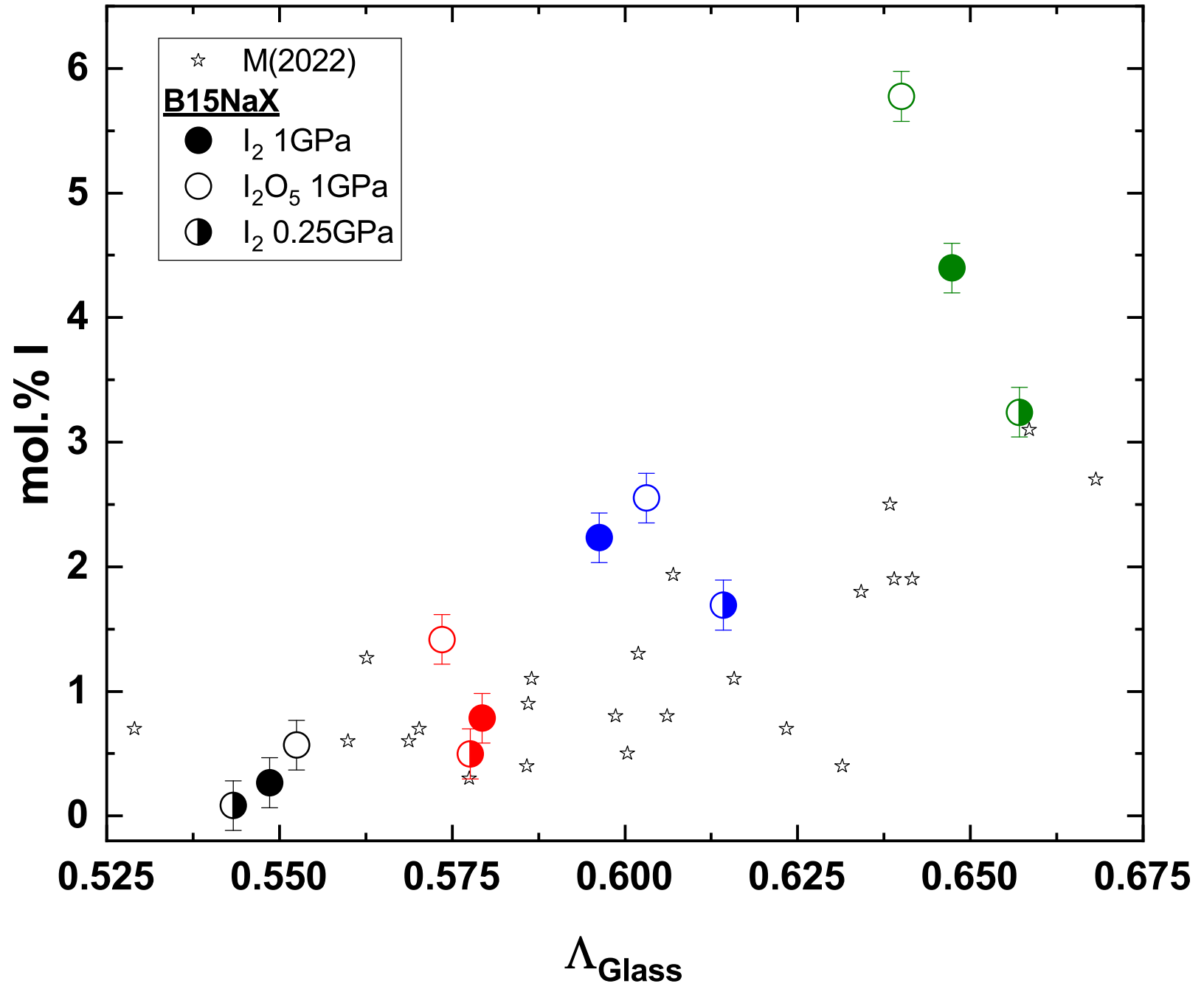
M(2022)
B15NaX
I2 1GPa
I2O5 1GPa
I2 0.25GPa
mol.% I
0
1
2
3
4
5
6
0.525
0.550
0.575
0.600
0.625
0.650
0.675
ΛGlass

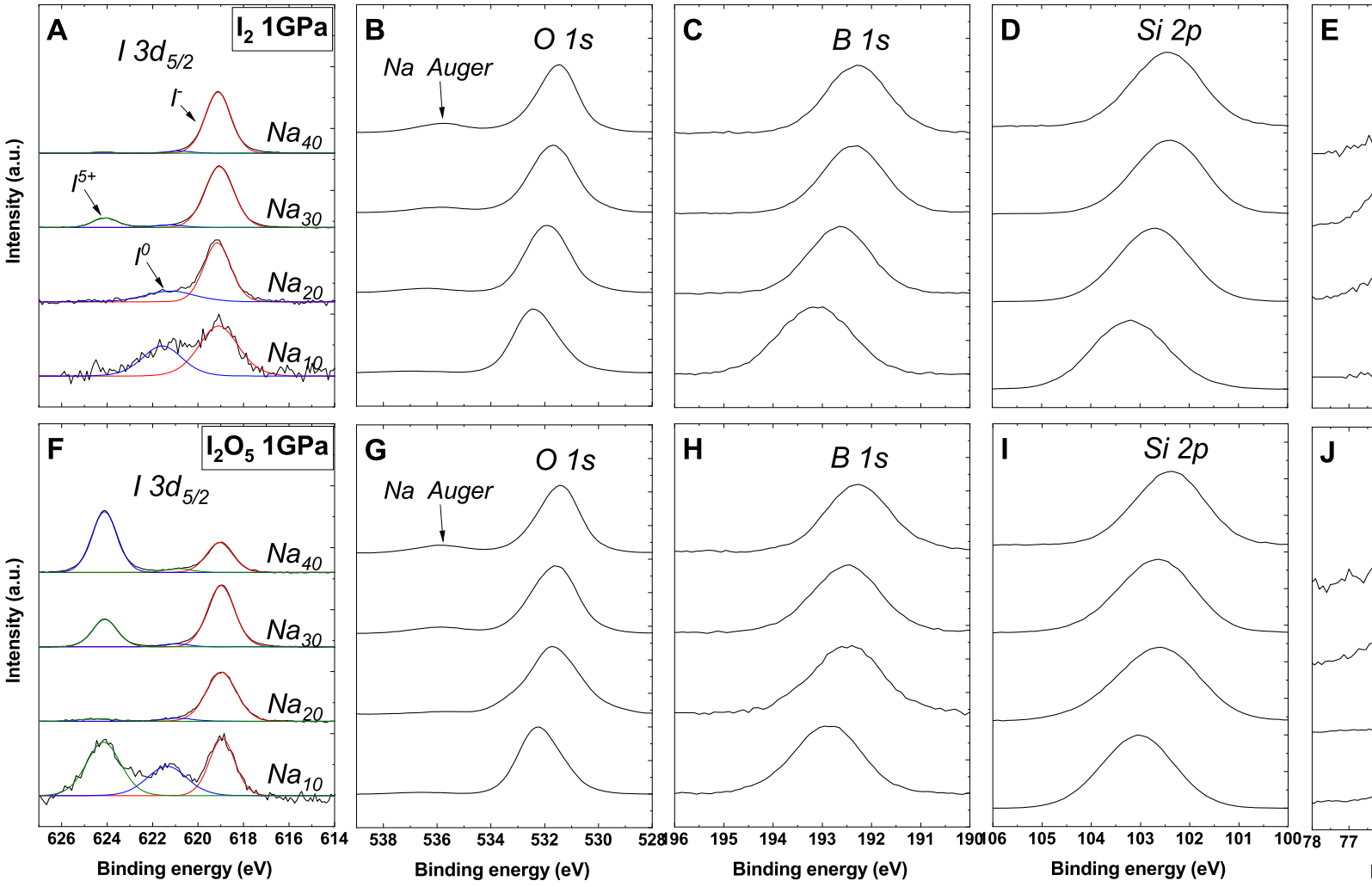
A
I2 1GPa
I 3d5/2
I-
Na40
I5+
Na30
I0
Na20
Na10
B
O 1s
Na Auger
C
B 1s
D
Si 2p
E
F
I2O5 1GPa
I 3d5/2
Na40
Na30
Na20
Na10
G
O 1s
Na Auger
H
B 1s
I
Si 2p
J
Intensity (a.u.)
Intensity (a.u.)
626 624 622 620 618 616 614
538 536 534 532 530 528
196 195 194 193 192 191 190
106 105 104 103 102 101 100
78 77
Binding energy (eV)
Binding energy (eV)
Binding energy (eV)
Binding energy (eV)

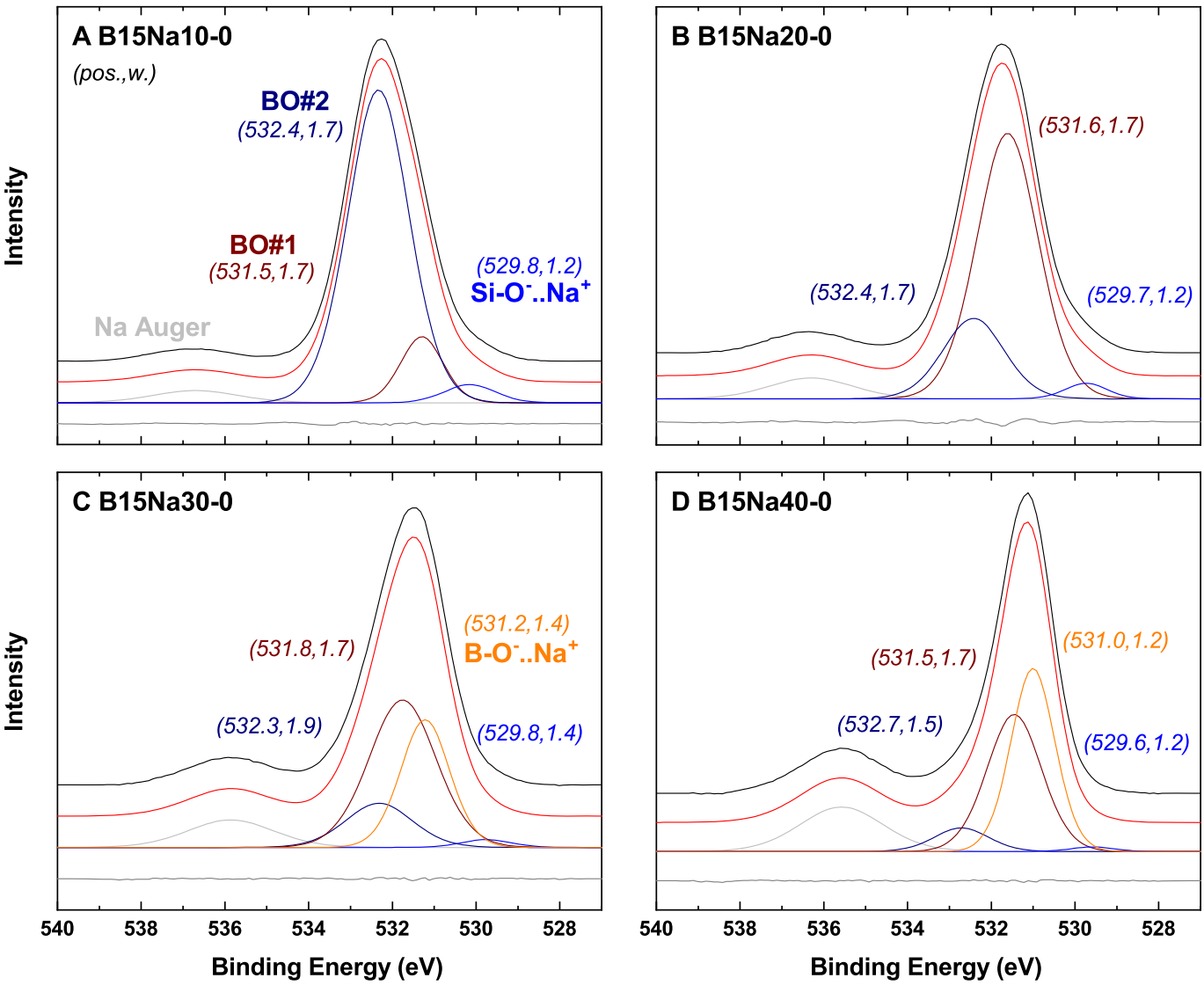
A B15Na10-0
(pos.,w.)
BO#2
(532.4,1.7)
BO#1
(531.5,1.7)
(529.8,1.2)
Si-O-..Na+
Na Auger
B B15Na20-0
(531.6,1.7)
(532.4,1.7)
(529.7,1.2)
C B15Na30-0
(531.8,1.7)
(531.2,1.4)
B-O-..Na+
(532.3,1.9)
(529.8,1.4)
D B15Na40-0
(531.5,1.7)
(531.0,1.2)
(532.7,1.5)
(529.6,1.2)
Intensity
Intensity
540
538
536
534
532
530
528
Binding Energy (eV)
Binding Energy (eV)

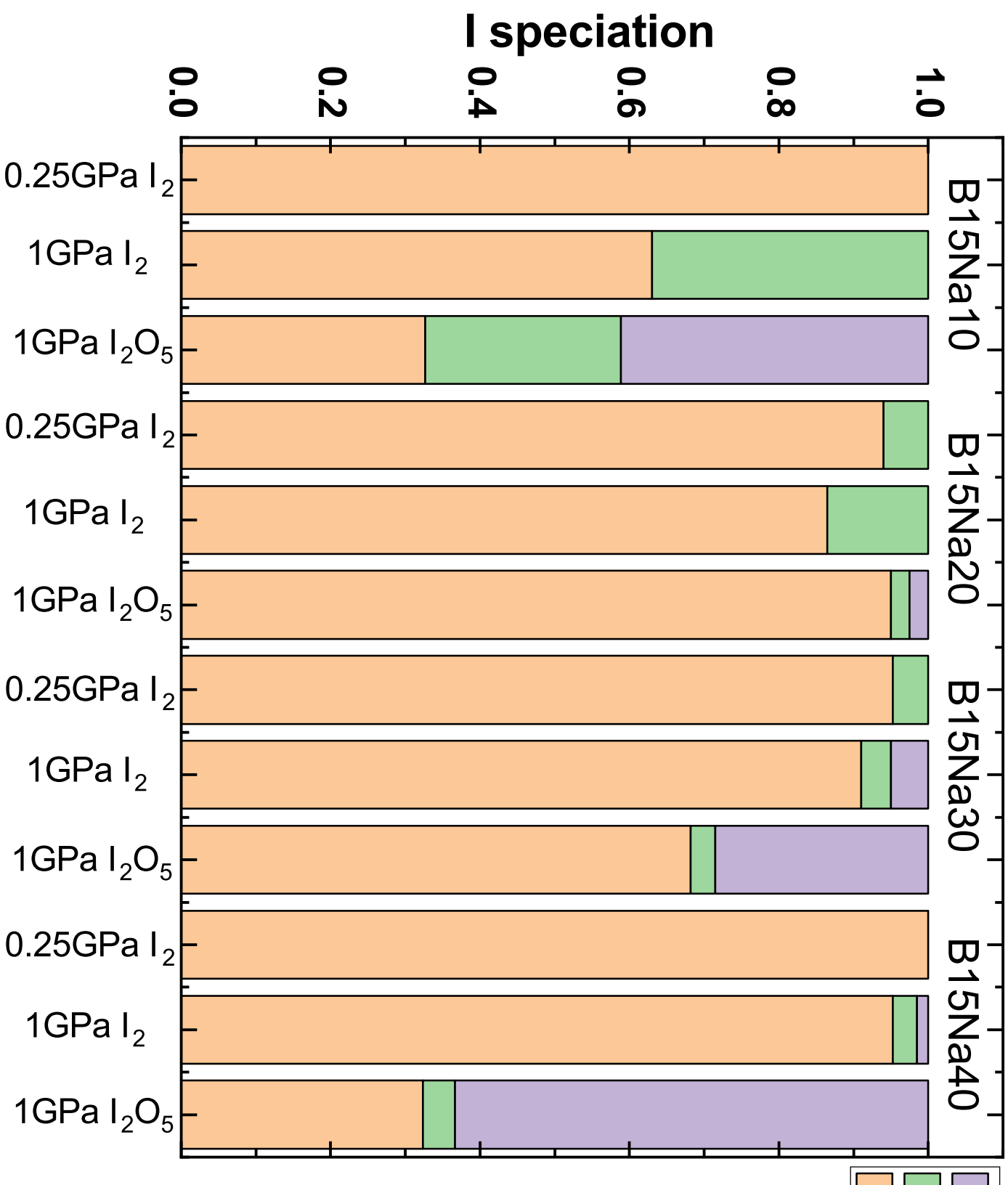
I speciation
0.0
0.2
0.4
0.6
0.8
1.0
0.25GPa I2
1GPa I2
1GPa I2O5
0.25GPa I2
1GPa I2
1GPa I2O5
0.25GPa I2
1GPa I2
1GPa I2O5
0.25GPa I2
1GPa I2
1GPa I2O5
B15Na10
B15Na20
B15Na30
B15Na40

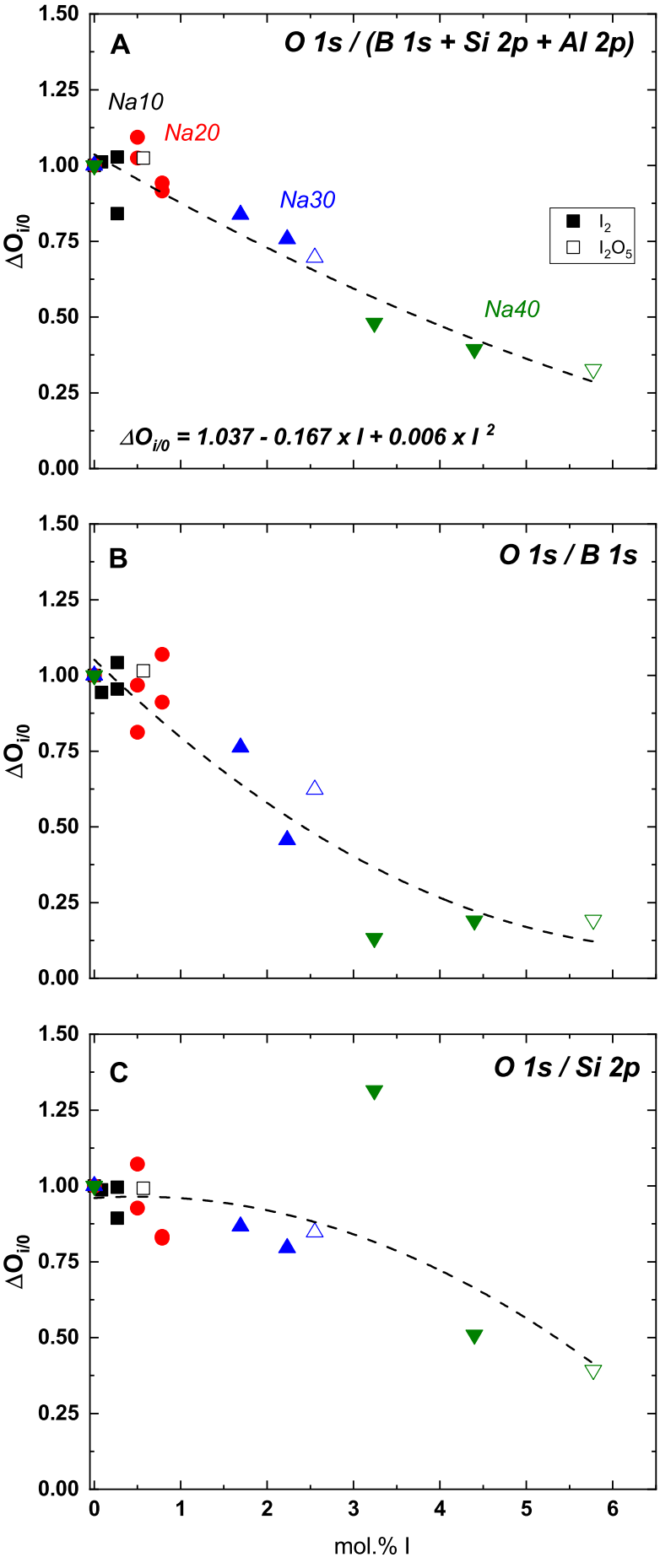
A
O 1s / (B 1s + Si 2p + Al 2p)
Na10
Na20
Na30
Na40
I2
I2O5
ΔOi/0 = 1.037 - 0.167 x I + 0.006 x I 2
B
O 1s / B 1s
C
O 1s / Si 2p
ΔOi/0
mol.% I
0.00
0.25
0.50
0.75
1.00
1.25
1.50
0
1
2
3
4
5
6

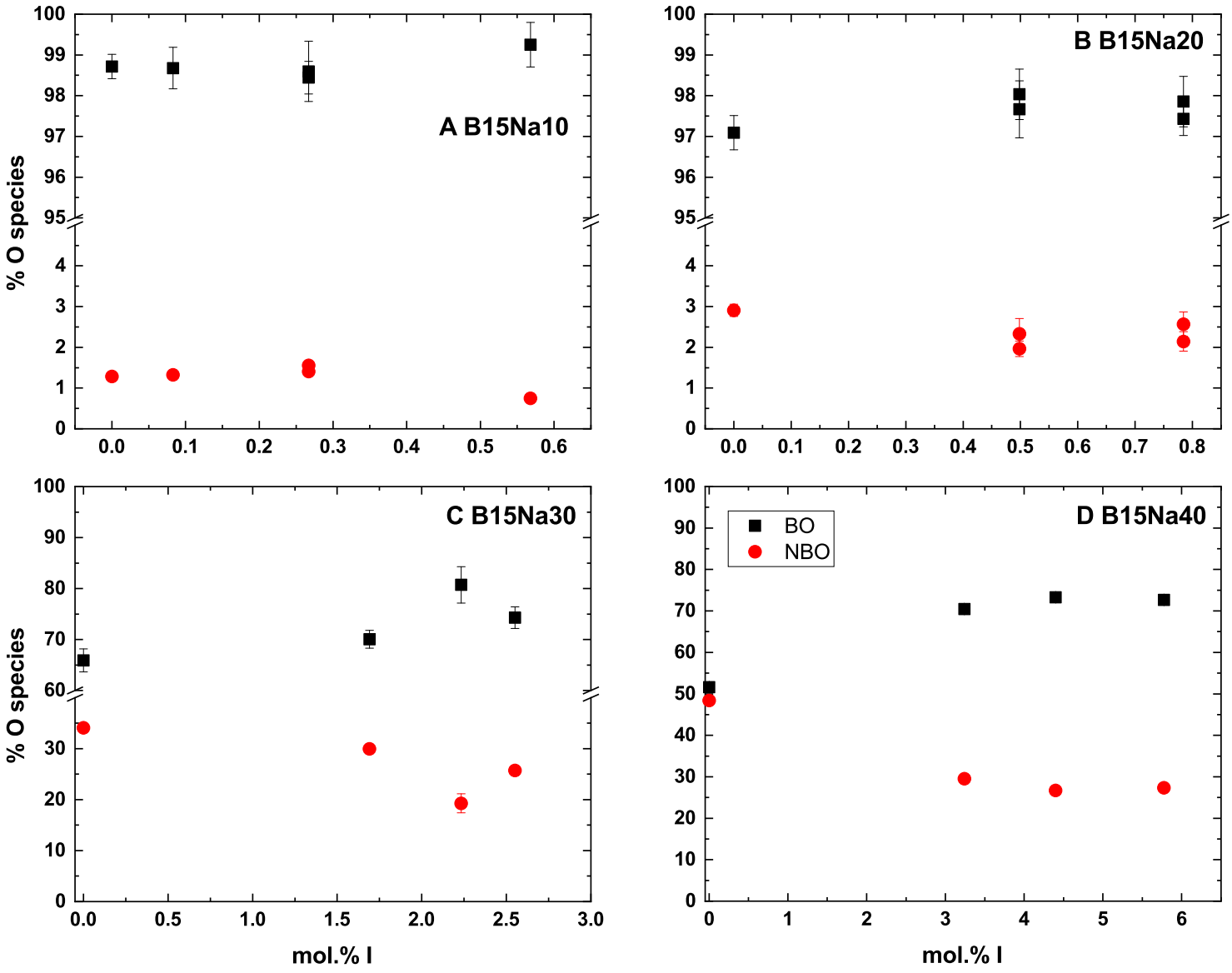
A B15Na10
B B15Na20
C B15Na30
D B15Na40
% O species
mol.% I
BO
NBO

SUPPLEMENTARY MATERIAL: IODINE DISSOLUTION MECHANISMS IN HIGH-PRESSURE BOROSILICATE NUCLEAR WASTE GLASSES AND ITS RELATIONSHIP TO OXYGEN SPECIATION

Scanning/Transmission Electron Microscopy (S/TEM) acquisition in I-bearing glasses

In order to investigate the presence of nanoparticles or nm-size bubbles filled with I_2 fluid in the glasses, we also conducted Scanning/Transmission Electron Microscopy (S/TEM) at 80 kV on a Cs probe corrected Themis Z G3 (Thermo Fisher Scientific) using the High Angle Annular Dark Field (HAADF) detector (with 33-197° collection angle range) and the 4-SDD detectors (Super-X system) for EDS analysis. Samples were previously prepared by dispersing the grinded powder in ethanol and depositing a drop of this solution on a holey-carbon-coated copper grid.

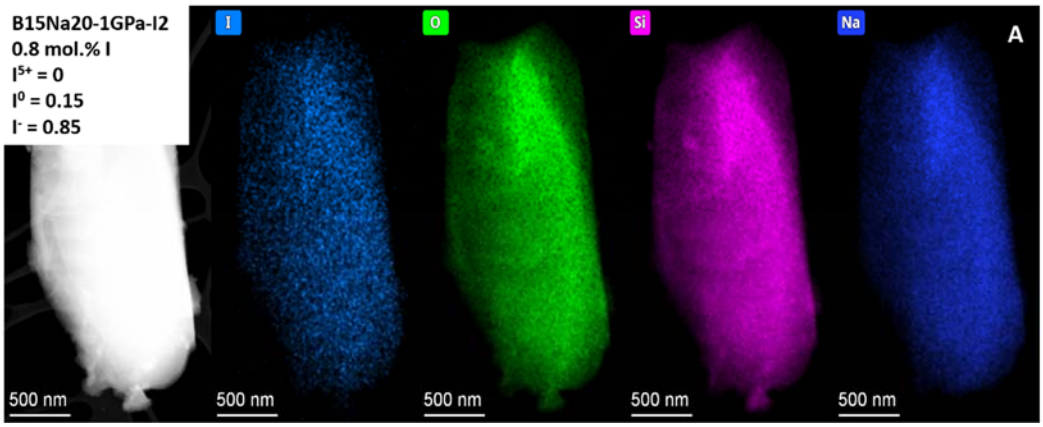

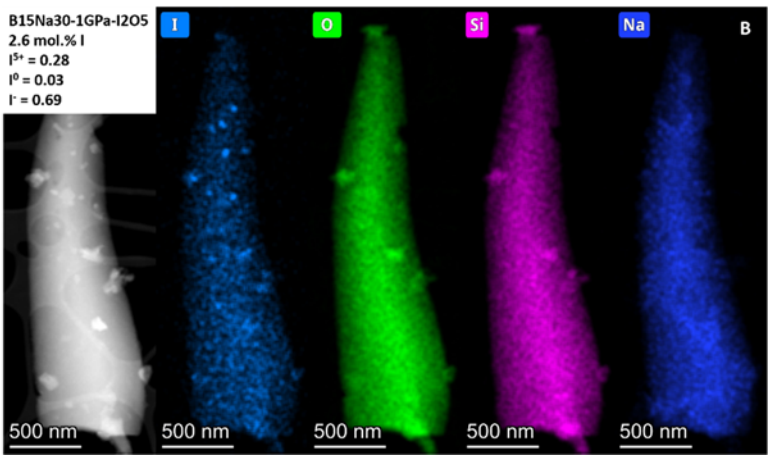

Figure S1: S/TEM element imaging for B15Na20-1GPa-I2 (A) and for B15Na30-1GPa-I2O5 (B). For both samples, the element distribution is homogeneous at the µm scale. We suspect the presence of nm-scale quenching crystal in B15Na30-1GPa-I2O5.

The elemental maps (I, O, Si and Na) are shown in Figure S1 for B15Na20-1GPa-I2 (A) and for B15Na30-1GPa-I2O5 (B). From the shown images, we observe that the obtained I-bearing glasses are homogeneous with respect to element distribution at µm scale. Clearly, we do not observe the presence of nm-scale bubble filled with solid I_2. This suggests that the presence of I^0 determined from XPS I 3d spectra corresponds to iodine dissolved within the glass structure as I^0 and probably under I_2 cluster form.

Whereas the presence of quench crystals has been identified in B15Na30 glasses, in Figure S1B, there is no clear evidence of large enriched iodine crystalline phases at the investigated scale. This implies that the quench crystals are not highly represented in our quenched samples.

Oxides	B15Na20-1GPa-I2		B15Na30-1GPa-I2O5	
	SEM EDS	S/TEM	SEM EDS	S/TEM
SiO_2 (mol.%)	62.6(2)	65.1(100)	58.1(6)	58.6(31)
B_2O_3	14.2(1)	14.2(1)	14.1(1)	14.1(1)
Al_2O_3	6.0(1)	5.7(11)	6.2(1)	5.5(5)
Na_2O	18.4(3)	14.3(27)	26.0(7)	20.3(9)
I	0.8(2)	0.8(1)	2.6(2)	1.5(3)

Table S1: Major element concentrations obtained by SEM EDS and S/TEM for B15Na20-1GPa-I2 and for B15Na30-1GPa-I2O5. The error bars are determined from replicated measurements for both methods. The I content derived by both analytical methods is roughly consistent.

The glass compositions have been obtained from the sample analyses in Figure S1. The results are given in Table S1 and compared to the results obtained from SEM EDS measurements. It should be pointed out that the error obtained on B15Na20-1GPa-I2 is based

on a single measurement whereas the error obtained on B15Na30-1GPa-I2O5 is based on four replicated measures. Although the error bars derived from the S/TEM are likely to be larger than SEM EDS ones, the measured mol.% oxides are consistent. The Na_2O is systematically lower for S/TEM measurements than for SEM EDS. The derived iodine content in B15Na30-1GPa-I2O5 is lower by S/TEM than SEM EDS. This could be due to possible heterogeneity within this sample.

O 1s XPS fitting for B15Na20-1GPa-I2O5

As mentioned in the manuscript, we have observed a very peculiar behavior for B15Na20-1GPa-I2O5. The O 1s XPS spectrum obtained for this sample is shown in Figure S2. If the spectrum simulation appears consistent with the general trend shown in Figure 4, the O 1s spectrum for B15Na20-1GPa-I2O5 departs from this trend. Clearly, there is a need for an additional peak to reproduce the entire spectrum. This peak is located at ~533 eV. It is not clear to which type of oxygen species this peak is attributed to. Malfait[1] suggested that at high binding energy, the peak could correspond to hydrated related species. Surprisingly, this sample is the only one to not show the presence of iodate species (I^{5+}). It could be possible that the I_2O_5 dissociation into I_2 and O_2 led to the incorporation of both I_2 as I^- or I^0 and O_2 without the recombination into IO_3^- clusters. The question remains to be clarified.

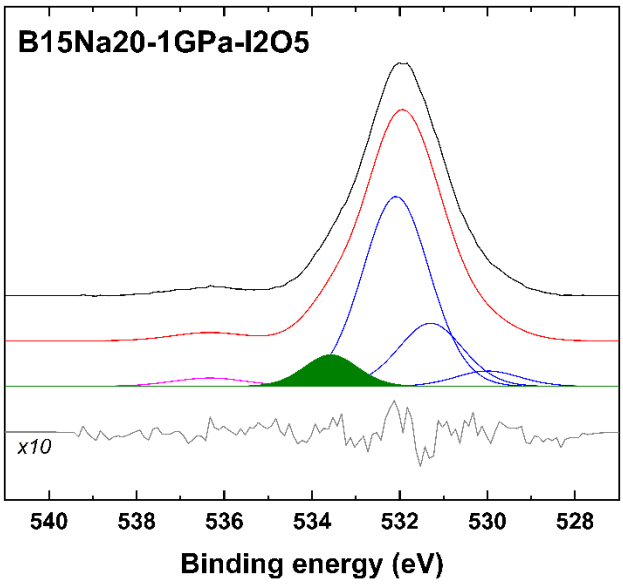

Figure S2: Typical simulations for B15Na20-1GPa-I2O5 glass. The simulation for B15Na20-1GPa-I2O5 requires an additional peak located at >533 eV and possibly attributed to hydrated oxygen species.

Reference:

[1] W. J. Malfait, *Can. J. Chem.*, 2015, **93**, 578-580.